Acta Pharmaceutica Sinica B 2026;16(5):2964−2981

Chinese Pharmaceutical Association
Institute of Materia Medica, Chinese Academy of Medical Sciences

Acta Pharmaceutica Sinica B

www.elsevier.com/locate/apsb
www.sciencedirect.com

ORIGINAL ARTICLE

Reblastatin as a neuroprotective agent in temporal lobe epilepsy and excitotoxic conditions of Alzheimer's disease and Parkinson's disease

Xiuneng Zhang[a,†], Xiaolin Yu[a,†], Longze Sha[a,c,f,†], Yunfeng Li[b], Qi Qiao[d,e], Xiaoming Yu[b,*], Qi Xu[a,f,*]

[a]*State Key Laboratory of Common Mechanism Research for Major Diseases, Department of Biochemistry and Molecular Biology, Institute of Basic Medical Sciences, Chinese Academy of Medical Sciences and Peking Union Medical College, Beijing 100005, China*
[b]*State Key Laboratory of Bioactive Substance and Function of Natural Medicine, Institute of Materia Medica, Chinese Academy of Medical Sciences and Peking Union Medical College, Beijing 100050, China*
[c]*State Key Laboratory of Complex, Severe and Rare Diseases, Peking Union Medical College Hospital, Peking Union Medical College and Chinese Academy of Medical Sciences, Beijing 100730, China*
[d]*Key Laboratory of Clinical Neurology, Ministry of Education, Hebei Medical University, Shijiazhuang 050000, China*
[e]*Department of Neurology, The Second Hospital of Hebei Medical University, Shijiazhuang 050000, China*
[f]*Neuroscience Center, Chinese Academy of Medical Sciences, Beijing 100005, China*

Received 22 October 2025; received in revised form 7 December 2025; accepted 16 December 2025

KEY WORDS

Reblastatin;
Hsp90;
EAAT2;
Glutamate;
Epilepsy;
Alzheimer's disease;

Abstract Previous studies have shown that heat shock protein 90 (Hsp90) inhibitors can reduce seizures in temporal lobe epilepsy (TLE) by upregulating excitatory amino acid transporter 2 (EAAT2, also known as GLT-1). While the Hsp90 inhibitor 17-AAG is effective, its long-term use raises toxicity concerns. This study aimed to identify a safer Hsp90 inhibitor by screening benzenoid ansamycin derivatives for higher binding affinity and lower toxicity. Among nine natural benzenoid ansamycins and their derivatives screened, reblastatin emerged as the top candidate, exhibiting the highest binding affinity to Hsp90. Compared to geldanamycin and 17-AAG, reblastatin demonstrated significantly lower

*Corresponding authors.
E-mail addresses: mingxyu@imm.ac.cn (Xiaoming Yu), xuqi@pumc.edu.cn (Qi Xu).
[†]These authors made equal contributions to this work.
Peer review under the responsibility of Chinese Pharmaceutical Association and Institute of Materia Medica, Chinese Academy of Medical Sciences.

https://doi.org/10.1016/j.apsb.2026.02.017

Parkinson's disease;
Excitotoxicity

cytotoxicity in HEK293 and HepG2 cells. Like 17-AAG, reblastatin upregulated EAAT2 levels by disrupting the association among Hsp90, EAAT2, and the 20S proteasome. In a kainic acid-induced TLE mouse model, reblastatin reduced seizure frequency by 50%, with long-term treatment showing toxicity comparable to vehicle controls. Additionally, behavioral tests revealed neuroprotective effects of reblastatin in mouse models of Alzheimer's disease and Parkinson's disease. These findings collectively suggest that reblastatin is a promising Hsp90 inhibitor for treating TLE and excitotoxic conditions associated with neurodegenerative diseases.

1. Introduction

Epilepsy is a neurological disorder caused by abnormal synchronous firing of neurons. It is one of the most prevalent neurological disorders, currently affecting approximately 50 million people worldwide, with the number expected to rise in the coming years[1]. Despite the availability of around 30 antiepileptic medicines, these medications are only statistically effective in about 60%−70% of patients[2,3]. Additionally, more than half of those on antiepileptic treatment still experience seizures, which often progress to drug-resistant epilepsy[4].

Temporal lobe epilepsy (TLE) with hippocampal sclerosis represents the most common form of drug-resistant epilepsy in adults. A hallmark of this condition is impaired astrocytic glutamate clearance, leading to excessive extracellular glutamate accumulation. This elevated glutamate level promotes neuronal hyperexcitability and seizure initiation[5,6].

Among the glutamate transporters, excitatory amino acid transporter 2 (EAAT2, gene symbol: *SLC1A2*, the human ortholog of mouse GLT-1. For clarity, we refer to the protein as EAAT2 throughout, corresponding to mouse GLT-1 and human EAAT2.) has been identified as a promising therapeutic target for TLE[7]. As the predominant glutamate transporter in the human adult brain, EAAT2 is responsible for clearing nearly 90% of glutamate from the synaptic cleft[8]. A significant reduction in EAAT2 protein levels is a pathological feature not only of TLE but also of other neurological disorders, including Alzheimer's disease (AD), Parkinson's disease (PD), and tuberous sclerosis[9-13]. Such deficits lead to extracellular glutamate accumulation, which, in turn, causes excitotoxicity, resulting in abnormal neuronal discharge and neurodegeneration[14].

Our previous studies have shown that upregulation of heat shock protein 90 (Hsp90) in reactive astrocytes promotes the 20S proteasome-dependent degradation of EAAT2. The geldanamycin (GA) derivative 17-AAG effectively disrupts the interaction between Hsp90 and EAAT2, thereby preventing EAAT2 degradation and exerting antiepileptic effects[15,16].

Benzenoid ansamycins and their derivatives represent a significant class of Hsp90 inhibitors, primarily developed as cancer treatments[17]. However, despite extensive research, no Hsp90 inhibitor has been approved by the US food and Drug Administration (FDA) for single-agent clinical cancer treatment. Hepatotoxicity remains the primary factor limiting the efficacy of these inhibitors[18]. GA, the first Hsp90 inhibitor isolated from the bacterium *Streptomyces hygroscopicus*[19], binds to the ATP-binding site in the N-terminal domain of Hsp90[20]. In preclinical studies, GA exhibited significant hepatotoxicity[21], leading to the development of less toxic and more soluble benzenoid ansamycins, such as 17-AAG. Although 17-AAG showed promise in Phase II trials, particularly in the treatment of HER2/ERBB2-positive trastuzumab-refractory breast cancer[22], its development was ultimately halted, underscoring the urgent need for less toxic derivatives. Biochemical studies suggest that the quinone moiety present in GA, 17-AAG, and their derivatives contributes to cellular cytotoxicity[23]. Consequently, the inhibitory effects observed with benzoquinone ansamycins in cancer cells are attributed to both the target moiety (which inhibits Hsp90) and the quinone moiety[18]. However, the antiepileptic activity of Hsp90 inhibitors is believed to result solely from their Hsp90 inhibitor activity. Therefore, we propose that nonquinone benzenoid ansamycins are more suitable candidates for further development as antiepileptic medicine.

In this study, we conducted computerized virtual screening and experimental verification of nine natural benzenoid ansamycin products and derivatives. Our findings revealed that the nonquinone benzenoid ansamycin reblastatin exhibited the highest binding affinity for Hsp90, along with lower cytotoxicity and hepatotoxicity compared to GA and 17-AAG. Moreover, it exhibited comparable multi-system toxicity to the control group. Notably, reblastatin administration significantly reduced the number of spontaneous seizures in a mouse model of TLE. It also shows promise in alleviating symptoms of PD and AD in mouse models.

2. Materials and methods

2.1. Reagents

Kainic acid (KA, 420318-10 MG), Pentetrazol (PTZ, P6500-25G), L-glutamic acid (G8415-100G), Carbamazepine (CBZ, C4024), and poly-D-lysine (PDL, P6407) were purchased from Sigma−Aldrich (Saint Louis, MO, USA). Cycloheximide (CHX, HY-12320), 17-AAG (HY-10211), GA (HY-15230), and memantine (HY-B0591) were purchased from MedChemExpress (Shanghai, China). Additional Hsp90 inhibitor compounds were provided by the Institute of Materia Medica, Chinese Academy of Medical Sciences, and Peking Union Medical College (Beijing, China). All chemical compounds were dissolved according to the manufacturer's instructions and applied at the specified concentrations.

2.2. Animals

Adult male C57BL/6J mice, CD-1 mice, Sprague−Dawley (SD) rats, and newborn C57BL/6J mice were obtained from Beijing Vital River Laboratory Animal Technology (Beijing, China). *Appswe/Ps1dE9* transgenic (APP/PS1) mice were acquired from

Suzhou Cyagen Biosciences Co., Ltd. (Suzhou, China). All the mice were handled according to protocols approved by the Institutional Review Boards of the Chinese Academy of Sciences and Peking Union Medical College (No. ACUC-A02-2019-003) and in accordance with the Guidelines for the Care and Use of Laboratory Animals of the Beijing Laboratory Animal Management Office.

2.3. Isolation and primary culture of astrocytes

Astrocytes were isolated from the cerebral cortices of newborn C57BL/6J pups and cultured according to a previously established protocol[24]. Cerebral cortices were harvested, mechanically dissociated, and suspended in DMEM (CM15019, Macgene, Beijing, China) supplemented with 20% FBS (F8687, Sigma−Aldrich) and 1% penicillin−streptomycin (CC004, Macgene). The cell suspension was then seeded onto PDL-coated culture dishes and incubated at 37 °C in a humidified atmosphere with 5% CO_2. Once the astrocytes reached confluence, microglia and oligodendrocytes were removed by gently blowing the bottom of the culture dish with a pipette. The purified astrocytes were then transferred to PDL-coated culture dishes for subsequent experiments.

2.4. Microscale thermophoresis (MST)

Recombinant Hsp90 (ab48801, Abcam, Cambridge, UK) was labeled using a His-Tag Labeling Kit (MO-L018, Nanotemper Technologies, Munich, Germany) and diluted to the specified concentration according to the manufacturer's instructions. Hsp90 inhibitor compounds were also diluted to the indicated concentration in PBST containing 2% DMSO (D2650, Sigma−Aldrich). Equal volumes of the labeled protein and diluted compounds were mixed at room temperature. The mixtures were then loaded into capillaries (MO-K022, Nanotemper Technologies) and analyzed using a Monolith NT115 (Nanotemper Technologies) device set to medium MST power and 60% excitation power. All experiments were performed in triplicate, and the data were analyzed using MO Affinity analysis software for data fitting.

2.5. Surface plasmon resonance

The binding affinity between reblastatin and the following proteins was measured by Biacore 8 K (Cytiva, Marlborough, MA, USA): Human HSP90 (H36-54H, SinoBiological, Beijing, China), Human HSP60 (HYP73917, MedChemExpress), Human HSP70/HSPA1A (HYP74877, MedChemExpress), Human HSP90B1 (HYP703226, MedChemExpress), Human TNF receptor-associated protein 1 (TRAP1, HYP71537, MedChemExpress), HSP40/DNAJB1 (HYP70331, MedChemExpress), Human HSPB8 (HYP70933, MedChemExpress). During each binding cycle, different concentrations of reblastatin flowed through the CM5 chip (Cytiva, BR100530). The results were fitted to a 1:1 Langmuir binding model using Biacore Insight software (Cytiva) to obtain the binding and dissociation constants.

2.6. Cellular thermal shift assay

HEK293 cells were lysed in PBS supplemented with protease inhibitor cocktail (B14001, Selleck, Houston, USA) using 3 freeze-thaw cycles, followed by centrifugation at 15,000 × *g* for 15 min at 4 °C. The supernatant protein concentration was quantified using the BCA method and normalized to 2 μg/μL. Equal aliquots were then dispensed into 1.5 mL tubes: one was treated with reblastatin (100 nmol/L) for 1 h at room temperature, while the control group received an equivalent volume of DMSO. Subsequently, equivalent aliquots from each group were distributed into PCR tubes and subjected to thermal denaturation for 10 min at specified temperatures (37−85 °C) using a PCR device (Bio-Rad, CA, USA). Following denaturation, samples were centrifuged at 20,000 × *g* for 20 min at 4 °C to pellet heat-denatured proteins, and the supernatants were collected for Western blot analysis. The following antibodies were used at the specified dilutions: Hsp90 (Rabbit, 13171-1-AP, 1:20,000, Proteintech, Wuhan, China), *β*-actin (Rabbit, 4970, 1:100,000, Cell Signaling Technology, Danvers, MA, USA). HRP-conjugated AffiniPure goat anti-rabbit (SA00001-2, 1:5000, Proteintech).

2.7. Molecular docking

The structures of all compounds were drawn using ChemDraw Professional 15.1, subjected to energy minimization with Chem3D 15.1, and hydrotreated with Sailvina. The crystal structure of Hsp90 (PDB ID: 1OSF) was downloaded from the Protein Data Bank and imported into PyMOL, where water molecules and other ligands were removed to generate a clean PDB file. The prepared molecule was then hydrotreated in AutoDockFR. The molecular structures of the proteins and compounds were converted to PDBQT format using Sailvina software. The binding site coordinates were determined with reference to the molecule KOS, isolated from the protein crystal structure. Molecular docking was performed using Sailvina, with docking parameters set to an exhaustiveness of 120, num modes of 60, and an energy range of 3. The docking results were evaluated based on docking scores and visualized in PyMOL software.

2.8. Extracellular glutamate uptake assay

Astrocytes were cultured in a 12-well plate and treated with 100 nmol/L GA, 17-AAG, or reblastatin for 36 h. Following treatment, the medium was replaced with glutamate-free DMEM (CM15018, Macgene) containing 2% FBS (16000, Gibco, Carlsbad, CA, USA), and the astrocytes were cultured for an additional 12 h to deplete intracellular glutamate. The medium was then removed, and the cells were washed twice with PBS (CC008, Macgene). Subsequently, medium containing 20 μmol/L glutamate was immediately added to each well. Supernatant samples (100 μL) were collected at 20, 40, and 80 min for further analysis. The glutamate concentration in each sample was measured using a glutamate assay kit (STA-674, Cell Biolabs, San Diego, CA, USA) following the manufacturer's protocol.

2.9. Cytotoxicity assay

HEK293 cells, HepG2 cells, and astrocytes were cultured at 37 °C in a humidified atmosphere of 5% CO_2. Upon entering the logarithmic growth phase, cells were harvested and resuspended at 3×10^4 cells/mL (HEK293 and HepG2) and 5×10^4 cells/mL (astrocytes). Aliquots of 100 μL of each cell suspension were seeded into 96-well plates and incubated for 24 h. Subsequently, the cells were treated with the test compounds at concentrations ranging from 0.005 to 50 μmol/L for 48 or 72 h. Finally, cell viability was assessed using a CCK-8 assay kit (HY-K0301, MedChemExpress).

2.10. Western blotting

Total protein was extracted using either Cell Lysis Reagent (C2978, Sigma−Aldrich) or lysis buffer (4% SDS, 100 mmol/L Tris). The following primary antibodies were used at the specified dilutions: Hsp90 (13171-1AP, 1:20,000, Proteintech), EAAT2 (sc-365634, 1:15,000, Santa Cruz, Dallas, TX, USA), GLT-1 (22515-1-AP, 1:30,000, Proteintech), FLAG (F1804, 1:1000, Sigma−Aldrich), Hsp90AB1 (11405-1-AP, 1:5000, Proteintech), 20S Proteasome (ab242061, 11,000, Abcam) and β-actin (4970, 1:100,000, Cell Signaling Technology). Secondary antibodies included goat anti-mouse (31430, 1:5000, Invitrogen, Eugene, OR, USA) and HRP-conjugated AffiniPure goat anti-rabbit (SA00001-2, 1:5000, Proteintech). Band intensities were quantified using ImageJ, with β-actin serving as the internal control for data normalization, and relative fold changes for each group were calculated.

2.11. Immunoprecipitation

The cellular lysates were clarified by centrifugation at 12,000 $\times$ *g* for 10 min at 4 °C. For immunoprecipitation assays, 0.7−1.2 mg of protein lysate was incubated with specific primary antibodies at 4 °C overnight with constant agitation. Protein complexes were then captured by incubation with Protein G Sepharose beads (ab193259, Abcam) for 2 h at 4 °C. Following three washes with PBS, immunoprecipitated proteins were recovered from the beads by boiling for 10 min in sample buffer or by competition with the tag peptide and then analyzed by immunoblotting.

2.12. Quantitative PCR

Total RNA was extracted from the hippocampus of normal and TLE mice using the RNeasy Mini Kit (74104, Qiagen, Venlo, Netherlands) according to the manufacturer's protocol. The cDNA was prepared using Fast Lane Cell cDNA Kit (21501, Qiagen). Levels of mRNA were assessed by real-time PCR using LightCycler 480 SYBR Green I Master (04707516001, Roche, Basel, Switzerland). A fragment of actin was amplified as the internal control. The following forward (F) and reverse (R) primers were used to amplify EAAT2 and actin: EAAT2 (F): 5′-TAGATATGTCGGTTGCCGTTTG-3′, EAAT2 (R): 5′-AGCCC AGTCCACCAGTGAGG-3′; Actin (F): 5′-GAGATTACTGC CCTGGCTCCTA-3′, Actin (R): 5′-TCATCGTACTCCTGCTTGC TGAT-3′. Differences in gene expression were calculated using the 2-delta CT method and are presented as the relative fold change.

2.13. KA model of TLE and video-electroencephalogram (vEEG) analysis

Four weeks after the stereotactic injection of 200 ng kA (in 200 nL PBS) into the dorsal hippocampal CA1 region (AP: −2.0 mm; ML: −2.0 mm; DV: −1.8 mm), the KA-induced TLE model was established, and wired vEEG recordings were conducted and analyzed as previously described[15]. Continuous vEEG monitoring for seizure activity began on Day 28 post-injection and continued for 15 days (baseline), commencing once spontaneous recurrent seizures were reliably observed. The mice experiencing at least four seizures per week were selected and then randomly divided into 2 groups: the vehicle group and the drug administration group. In this model, seizure frequency increases progressively over time, a phenomenon well-documented in previous studies[25−27], simulating the process of temporal lobe epileptogenesis. The classic antiepileptic drug CBZ was administered *via* intraperitoneal (i.p.) injection at a dose of 40 mg/kg/day to evaluate its long-term pharmacological effects for 4 weeks. The treatments with reblastatin were administered every other day, with 16 mice in the vehicle group and 19 mice in the drug administration group. vEEG continuously monitored epileptic seizures for 25 days following the initiation of treatment. Seizures in the EEG data were identified by bursts of high-amplitude vEEG activity, while limb clonus or generalized seizures were identified by two trained experimenters in a double-blinded manner.

APP/PS1 mice also underwent vEEG analysis following a one-week acclimation period. Baseline motor seizures were recorded over 14 consecutive days before vehicle or reblastatin treatment. The selected mice were then randomly divided into two groups: 8 in the vehicle group and 8 in the reblastatin group. Treatments were administered every other day. vEEG continuously monitored epileptic seizures for 14 days following the initiation of treatment.

2.14. Mouse model of PTZ-induced seizure

PTZ powder was dissolved in saline to prepare a stock solution of a specific concentration. After a 1-week acclimation period, C57BL/6J mice were administered PTZ (55 mg/kg, i.p.), and the onset time and seizure severity were recorded. The treatment group received 3 preliminary i.p. injections of reblastatin (1, 2, 4, and 10 mg/kg), while the control group was injected with DMSO. Seizure severity was assessed using the Racine score. Racine score criteria: (i) Score 0: no response; (ii) Score 1: facial clonus, including blinking, whisker twitching, and rhythmic chewing; (iii) Score 2: Score 1 plus forelimb clonus, without rearing; (iv) Score 3: Score 2 plus rearing; (v) Score 4: generalized tonic-clonic seizures with loss of postural control; (vi) Score 5: death.

2.15. Mouse model of MPTP-induced PD

MPTP (60388ES25, Yeasen Biotechnology, Shanghai, China) was dissolved in saline to prepare a stock solution, while probenecid (IP0380-500 MG, Solarbio, Beijing, China) was dissolved in DMSO to create its stock solution. Following a one-week acclimatization period in the barrier facility, C57BL/6J mice were randomly divided into two groups. The experimental group received i.p. injections of MPTP (25 mg/kg) and probenecid (250 mg/kg) twice weekly for 5 weeks. To optimize the effectiveness of chronic MPTP neurotoxicity, probenecid was administered 30 min before MPTP injections, serving as an adjuvant by reducing renal excretion of MPTP and its metabolites[28]. Reblastatin was administered simultaneously during the modeling period after being pre-administered twice. The experimental group received i.p. injections of reblastatin at 4 mg/kg every other day, while the control group received i.p. injections of DMSO. A total of 17 injections were administered. Behavioral assessments were conducted three days after the last injection.

2.16. Paraffin section immunofluorescence staining and quantification

Mice were deeply anesthetized with 0.7% pentobarbital sodium salt (P3761, Sigma−Aldrich) and subsequently perfused with 4% PFA (G1101, Servicebio, Wuhan, China). The brains were quickly removed, fixed in 4% PFA for at least 48 h, and then embedded in

paraffin wax. Paraffin-embedded tissues were sectioned at a thickness of 4 μm and mounted on glass slides coated with 0.5% gelatin (A609764-0100, Sangon Biotech, Shanghai, China). The following reagents were used: primary antibody against glial fibrillary acidic protein (GFAP, 3670S, 1:2,000, Cell Signaling Technology), anti-S100β antibody (ab52642, Abcam), Glutamine Synthetase Polyclonal antibody (11037-2-AP, Proteintech), Cleaved Caspase 3 Polyclonal antibody (25128-1-AP, Proteintech) and anti-β-3 Tubulin antibody (ab78078, Abcam), donkey anti-mouse IgG (H + L) highly cross-adsorbed secondary antibody (A-21202, Invitrogen), and DAPI (D9542, Sigma−Aldrich). All images were captured using a Leica fluorescence microscope, and staining was quantified with Leica X software.

2.17. Frozen section immunofluorescence staining and quantification

Mice were deeply anesthetized with 0.7% pentobarbital sodium salt (P3761, Sigma−Aldrich) and subsequently perfused with 4% PFA (G1101, Servicebio). The brains were quickly removed, fixed in 4% PFA for at least 48 h, and then transferred to 15% and 30% sucrose solution until the tissue sank to the bottom of the centrifuge tube. After fixation and dehydration, tweezers were used to carefully place the mouse brain onto the sample holder, ensuring that the brain tissue was thoroughly and evenly embedded in OCT. Once the tissue is positioned correctly, the sample was placed in a −80 °C freezer and allowed to solidify completely. OCT-embedded tissues were sectioned at a thickness of 10 μm and mounted on glass slides. The following reagents were used: primary antibody against tyrosine hydroxylase (TH, ab137869, 1:200, Abcam), donkey anti-rabbit IgG (H + L) highly cross-adsorbed secondary antibody (A-21206, 1:500, Invitrogen), and DAPI (D9542, Sigma−Aldrich). All images were captured using a Leica fluorescence microscope, and staining was quantified with Leica X software.

2.18. Evans blue staining

Three male mice with KA-induced chronic TLE and three age/sex-matched control mice were injected intravenously in the tail with 200 μL 2% Evans blue dye (E2129, Sigma, Darmstadt, Germany). The mice were euthanized after 12 h of dye circulation. Mice were perfused transcardially with PBS followed by 4% paraformaldehyde in PBS (0.1 mol/L, pH 7.4), cryoprotected in 15% and 30% sucrose solution, and embedded in OCT. Compound and frozen at −80 °C. Coronal slices of 40 μm were obtained by cryostat and mounted in Antifade Mounting Medium with DAPI (H-1200-10, Vector Labs, Burlingame, CA, USA). The slides were examined and photographed using a fluorescence microscope. Evans blue dye was observed in red (546 nm excitation filter), and nuclear DAPI staining was observed in blue.

2.19. Toxicity tests

Mice were randomly divided into seven groups and treated with vehicle (DMSO), 4 mg/kg GA, 20 mg/kg GA, 4 mg/kg 17-AAG, 20 mg/kg 17-AAG, 4 mg/kg reblastatin, or 20 mg/kg reblastatin. Each group received an i.p. injection of 50 μL of the respective reagent every other day for 2 weeks, with general conditions of the mice monitored throughout the treatment period. Body weight and liver weight were recorded to calculate the liver index, and paraffin-embedded sections were prepared for hematoxylin−eosin (HE) staining to evaluate liver morphology. Images were captured using a Leica fluorescence microscope. Serum samples were collected from the mice to measure levels of aspartate aminotransferase (AST, E-BC-K236-M), alanine aminotransferase (ALT, E-BC-K235-M), blood urea nitrogen (BUN, E-BC-K183-M), and creatinine (CREA, E-BC-K188-M) using kits from Elabscience (Wuhan, China).

To systematically assess the potential systemic toxicity of the 4 mg/kg dosing regimen, we performed long-term (3 months) toxicological evaluations. Each mouse received injections every other day, and the mice's general condition was monitored throughout the treatment period. The assessment protocol incorporated serum biochemical profiling and histopathological analysis of major organs (liver and kidney) using HE staining. One mouse in each group exhibited hemolysis, compromising the accuracy of their biochemical results; the hemolytic sample was consequently excluded from the final analysis. The serum biochemical evaluation encompassed three major panels: 1) hepatic function markers including ALT (S03030), AST (S03040), gamma-glutamyl transferase (γ-GT, S03031), total bilirubin (T-BIL, C120), direct bilirubin (D-BIL, C119), alkaline phosphatase (ALP/AKP, S03038), albumin (ALB, S03043) and total bile acids (TBA, S03074); 2) renal function parameters comprising BUN (S03036), CREA (S03076) and uric acid (UA, S03035); and 3) cardiac enzymes profile consisting of lactate dehydrogenase (LDH, S03034), lactate dehydrogenase isoenzyme 1 (LDH1, C058), creatine kinase (CK, S03024) and creatine kinase-MB isoenzyme (CK-MB, S03023). Appropriate assay kits were selected from Rayto (Shenzhen, China) and Changchun HuiLi Biotechnology Co., Ltd. (Changchun, China). Automated biochemical analysis was performed using a fully automated biochemistry analyzer (Chemray 240, Rayto, Shenzhen, China), including calibration, quality control, and sample measurement to determine target parameters.

2.20. Plasma stability test

Reblastatin was co-incubated with human plasma (KB122921-04-P001), dog plasma (KB040122-03-P001), mouse plasma (KB030122-01-P001), and rat plasma (KB051922-01-P001) purchased from 3D BioOptima (Suzhou, China) in a volume of 200 μL at a final concentration of 1 μmol/L. At various time points (0, 10, 30, 60, 90, and 120 min), 20 μL samples of the incubated plasma were collected and transferred into an appropriate volume of acetonitrile (A22T0218, ASTOON, Wilmington, Delaware, USA) containing the internal standard glibenclamide (L1920134, Shanghai Aladdin Biochemical Technology, Shanghai, China). Following protein precipitation, the supernatant was obtained by centrifugation. LC−MS/MS was then employed to analyze the ratio of analyte to internal standard peak areas, allowing calculation of the clearance constant, clearance half-life, and *in vitro* intrinsic clearance rate of reblastatin.

2.21. Plasma protein binding test

A stock solution of reblastatin was prepared and then diluted with a methanol:acetonitrile:water mixture (1:1:2, *v*/*v*/*v*) to create a working solution. The plasma protein binding of the compound across different species was assessed using equilibrium dialysis with a 96-well dialysis device (HTD96b, HTDialysis, Nieuwegein, Netherlands). Four microliters of the test solution were combined with 396 μL of plasma. For the control sample, 10 μL

of plasma was mixed with 90 μL of PBS containing 0.002% Tween 80 (H1611035, Shanghai Aladdin Biochemical Technology), then added to a precipitating solution containing the internal standard, glibenclamide. Subsequently, 150 μL of plasma and 150 μL of PBS were transferred to the test chamber and receiving chamber, respectively, on opposite sides of the dialysis membrane (9201251, HTDialysis).

The sample was incubated at 37 °C for 6 h. After incubation, 10 μL of the sample from the test chamber was added to 90 μL of phosphate buffer, thoroughly mixed, and then added to a precipitating solution containing the internal standard glibenclamide. In parallel, 90 μL of the sample from the receiving chamber was mixed with 10 μL of blank plasma from the same species, followed by the addition of the precipitating solution containing the internal standard glibenclamide. The remaining plasma samples were also incubated at 37 °C for 6 h. Subsequently, 10 μL of each sample was mixed with 90 μL of PBS, then added to the precipitating solution containing the internal standard, glibenclamide, to prepare stability samples.

2.22. Liver microsomal metabolism analysis

Reblastatin was co-incubated with liver microsomes from humans (1151001), dogs (074002), rats (0272002), and mice (1104001), along with the coenzyme NADPH (050001, Shanghai Regal Biology Technology, Shanghai, China). All liver microsomes were purchased from Corning (Corning, New York, NY, USA). At 0, 5, 15, 30, and 60 min, 20 μL of the incubation mixture was removed and transferred to 200 μL of acetonitrile containing an internal standard to terminate the reaction. After protein precipitation, the supernatant was obtained by centrifugation at 1944×*g* for 10 min. The supernatant was then diluted 1:1 with water and analyzed by LC−MS/MS. The *in vitro* clearance rate was calculated from the compound's elimination half-life. Midazolam (YZ5J-ZZX4, National Institutes for Food and Drug Control, Beijing, China) was used as a positive control.

2.23. In vivo pharmacokinetic analysis of reblastatin

The pharmacokinetic profile of reblastatin was evaluated in normal male SD rats and in male mouse models of TLE (4 weeks after kainic acid injection), AD (6-month-old APP/PS1 mice), and PD (MPTP-induced). Reblastatin was formulated in a vehicle of DMSO:PEG400:water (10:40:50, *v*/*v*/*v*). Animals received a single dose of reblastatin *via* i.p. injection (4 mg/kg), intravenous (i.v.) injection (2 mg/kg), or oral gavage (10 mg/kg). Whole blood samples were collected at designated time points into EDTA-K2 tubes and centrifuged at 1500×*g* to obtain plasma for drug concentration analysis. Concurrently, brain tissues were harvested at various time points, homogenized in 20% methanol−water, and analyzed for reblastatin content.

2.24. Animal behaviors

2.24.1. Open field test

It is used to assess locomotor behavior. A 50 cm × 40 cm × 40 cm square arena was used for the experiment. The open field area was evenly divided into 25 small squares, with the middle 9 squares designated as the central area and the remaining 16 squares as the peripheral area. The mouse was placed in the center of the arena to begin the test, allowing it to explore the environment freely. The movement trajectory was recorded using ANYMAZE video-tracking software. Each mouse was tested once for 5 min. During this time, record the total distance traveled and the time traveled in the central areas.

2.24.2. Pole test

It is designed to evaluate motor coordination in mice by observing their ability to grip and descend a vertical pole. The test apparatus consists of a wooden pole, 1 cm in diameter and 50 cm in length, with a 2.5 cm-diameter wooden ball securely fixed to the top. To prevent slippage during the descent, the pole is wrapped with gauze. During the test, the pole is raised at a 90° angle to the ground. The mouse is placed on the ball, and the time it takes to climb down spontaneously to the bottom of the pole is recorded. Each mouse undergoes three trials, with at least a 30-min interval between trials.

2.24.3. Wire hang test

A 50-cm-long, 2-mm-diameter steel wire was suspended 40 cm above the ground, with platforms at each end. Mice were placed on the wire's midpoint using their forepaws and observed for 30 s across 3 trials. Scoring was based on the following criteria: (i) Score 0: fell off; (ii) Score 1: hung on with 2 forepaws; (iii) Score 2: made attempts to climb while hanging on; (iv) Score 3: hung on with 2 forepaws and one or both hind paws; (v) Score 4: hung on with all four paws and the tail wrapped around the wire; (vi) Score 5: escaped to one of the platforms[29].

2.24.4. Novel object recognition test

Mice were first habituated to an empty arena. During the training phase, 2 identical objects were introduced, and the mice were allowed to explore them for 10 min. After a delay, one of the objects was replaced with a novel object, and the mice were given another 5 min to explore. The time spent exploring the novel object relative to the familiar one served as a measure of memory performance.

2.24.5. Y maze test

The apparatus consisted of three identical arms (35 cm long × 5 cm wide × 15 cm high) positioned at 120° angles. Mice were placed at the center and allowed to explore freely for 10 min. An arm entry was recorded when all four paws entered an arm. The percentage of spontaneous alternation was calculated as Eq. (1):

$$\text{Percentage of spontaneous alternation (\%)} = (\text{Number of alternations}/\text{Total arm entries} - 2) \times 100 \quad (1)$$

2.24.6. The elevated plus maze test

The elevated plus maze apparatus was used to evaluate anxiety-like behavior in PD mice. The apparatus consisted of two open arms (50 cm × 10 cm) crossed with 2 closed arms (50 cm long × 10 cm wide × 40 cm high). The maze was elevated 50 cm above the ground. The mice were placed in the laboratory for 1 h, then placed in the center of the maze, facing the open arm. The animal's behavior was recorded for 5 min using an overhead video-tracking system. The behavior of mice was recorded by an overhead tracking system (ANYMAZE software 5.11) for 5 min. The experiment was conducted in a quiet area away from other mice. During the experiment, the maze was cleaned with a 75% ethanol solution between trials, and the following experiment was

conducted after the alcohol evaporated. Finally, the number of times the mice entered the open and closed arms was counted, and the total time the mice spent in the open and closed arms was calculated, along with the percentage of time spent in the open and closed arms.

2.24.7. Morris water maze test

The Morris water maze test was conducted in a circular water-filled maze. There were some cues outside the maze to provide guidance, and their positions remained unchanged throughout the test. During the experiment, the animals' swimming paths were recorded by an overhead tracking system (ANYMAZE software 5.11) and stored on a computer. Pre-training was conducted 1 day before the hidden-platform test, during which the animals freely swam for 90 s without a platform. In the hidden-platform test, a transparent platform was placed 1 cm below the water level. Mice underwent 2 trials daily, with each trial randomly released from four directions, allowing the mice to swim freely for 60 s. Mice were allowed to rest on the platform for 10 s if they found the platform and were then placed in the home cage until the subsequent trial. Mice were guided to the platform to rest for 10 s if they failed to find it within 60 s. The escape latency of each mouse was calculated during the experiment. The hidden platform was removed during the probe trials, and each mouse was released from the same position and allowed to swim freely for 45 s. The time the mouse spent in the target zone where the platform was located was recorded. During the visible-platform test, the platform was placed above the water surface and positioned at different locations, and the latency time of each mouse was recorded.

2.25. Tandem mass tag (TMT)-based quantitative proteomic analysis

Mice received i.p. injections of reblastatin at 4 mg/kg every other day. Following three administrations, hippocampal tissues were harvested on the subsequent day. Proteins were extracted from the hippocampal tissues and enzymatically digested for further analysis. Isobaric labeling of peptides was performed using the 16-plex TMT reagents (A44520, ThermoFisher Scientific, Waltham, MA, US). TMT-labeled peptides were fractionated *via* basic reversed-phase chromatography on a RIGOL L-3000 dual gradient High-Performance Liquid Chromatography using an Agela Durashell-C18 column (4.6 mm × 250 mm i.d., 5 μm, 100 Å). The column oven was set at 45 °C with a flow rate of 0.7 mL/min. The solvent gradient was set as follows: 5% B, 0 min; 5%−8% B, 5 min; 8%−18% B, 35 min; 18%−32% B, 22 min; 32%−95% B, 6 min; 95%−5%, 4 min. The fractions collected were orthogonally concatenated into 10 pooled fractions. The tryptic peptide fractions were dissolved in buffer A (0.1% formic acid) and eluted at a flow rate of 600 nL/min with buffer B (80% acetonitrile and 0.1% formic acid). The Q Exactive HF-X mass spectrometer was used for LC−MS/MS analysis with a Nanospray Flex Ion Source (Thermo Fisher Scientific) and a spray voltage of 2.2 kV. The full MS scans were performed from *m*/z 350 to 1800 at a resolution of 60,000—normalized AGC target set to Standard and maximum injection time set to Auto. The MS/MS scans were performed at a resolution of 45,000, with a normalized AGC target of 100% and a maximum ion injection time of 120 ms. The collision energy was 34%. RAW files were analyzed using the Proteome Discoverer suite (version 3.1, ThermoFisher Scientific). MS^2 spectra were searched against the UniProt *Mus musculus* proteome database (54,822 target sequences downloaded on 7 March 2024). Percolator was used to filter peptide spectral matches and peptides to a false discovery rate of less than 1%. After spectral assignment, peptides were assembled into proteins and further filtered based on the combined probabilities of their constituent peptides, resulting in a final false discovery rate of 1%. Unique and razor peptides were considered for quantification. Proteins with adjusted *P* values less than 0.05 and fold changes greater than 1.5 or less than 0.66 were selected as differentially expressed proteins for further GO analysis.

2.26. Pharmacokinetic and statistical analysis

Statistical analysis was performed using Prism software version 9.0.0 (GraphPad). A *P* value of less than 0.05 was considered statistically significant. The pharmacokinetic profiles of reblastatin in mice and rats were analyzed using a non-compartmental model in Pharsight Phoenix 8.0. The results are presented as mean ± standard error of mean (SEM).

3. Results

3.1. Reblastatin shows a stronger binding affinity for Hsp90 and lower cytotoxicity

Hsp90 inhibitors with higher binding affinity may exhibit reduced hepatotoxicity when administered systemically. We first employed virtual screening methods to assess the docking scores of nine benzenoid ansamycins with Hsp90. These included 3 benzoquinone ansamycins (GA, 17-AAG, 17-DMAG), IPI-504 (a 17-AAG analog containing a reduced hydroquinone), the nonquinone benzenoid ansamycin reblastatin, and four of its derivatives (Fig. 1A). Western blotting analysis demonstrated that these compounds effectively increased EAAT2 levels in primary cultured astrocytes (Supporting Information Fig. S1). Notably, reblastatin and some of its derivatives exhibited superior docking scores compared to GA and 17-AAG (Fig. 1B). Binding conformation analysis revealed that the phenolic hydroxyl group at the 18-position of reblastatin is predicted to form an additional hydrogen bond with Gly97 in Hsp90, a feature absent in the GA-Hsp90 docking model (Fig. 1C and D). Compared to the 17AAG-Hsp90 docking model, the reblastatin-Hsp90 docking model also exhibits an additional hydrogen bond (Fig. 1E).

To validate the molecular docking results, we used MST to quantify the interactions between Hsp90 and three compounds: reblastatin, GA, and 17-AAG. The results confirmed that reblastatin binds to Hsp90 with a higher affinity (K_D = 3.43 nmol/L) than both GA and 17-AAG (Fig. 1F). This finding was corroborated by surface plasmon resonance assays, which showed a K_D value of 7.45 nmol/L (Supporting Information Fig. S2A). Furthermore, reblastatin exhibited higher specificity for Hsp90 than for 6 other heat shock proteins, including Hsp40, Hsp60, Hsp70, HspB1, TRAP1, and Hsp90B1 (Supporting Information Fig. S2B−S2G and Table S1). To evaluate target engagement *in vitro*, we employed the cellular thermal shift assay. Reblastatin-treated HEK293 cells showed a significant increase in thermally stabilized Hsp90, demonstrating that reblastatin directly binds to Hsp90 (Fig. S2H and S2I).

To determine whether the 18-position phenolic hydroxyl substitution in reblastatin contributes to reduced cytotoxicity, we assessed the inhibitory effects of reblastatin, GA, and 17-AAG on

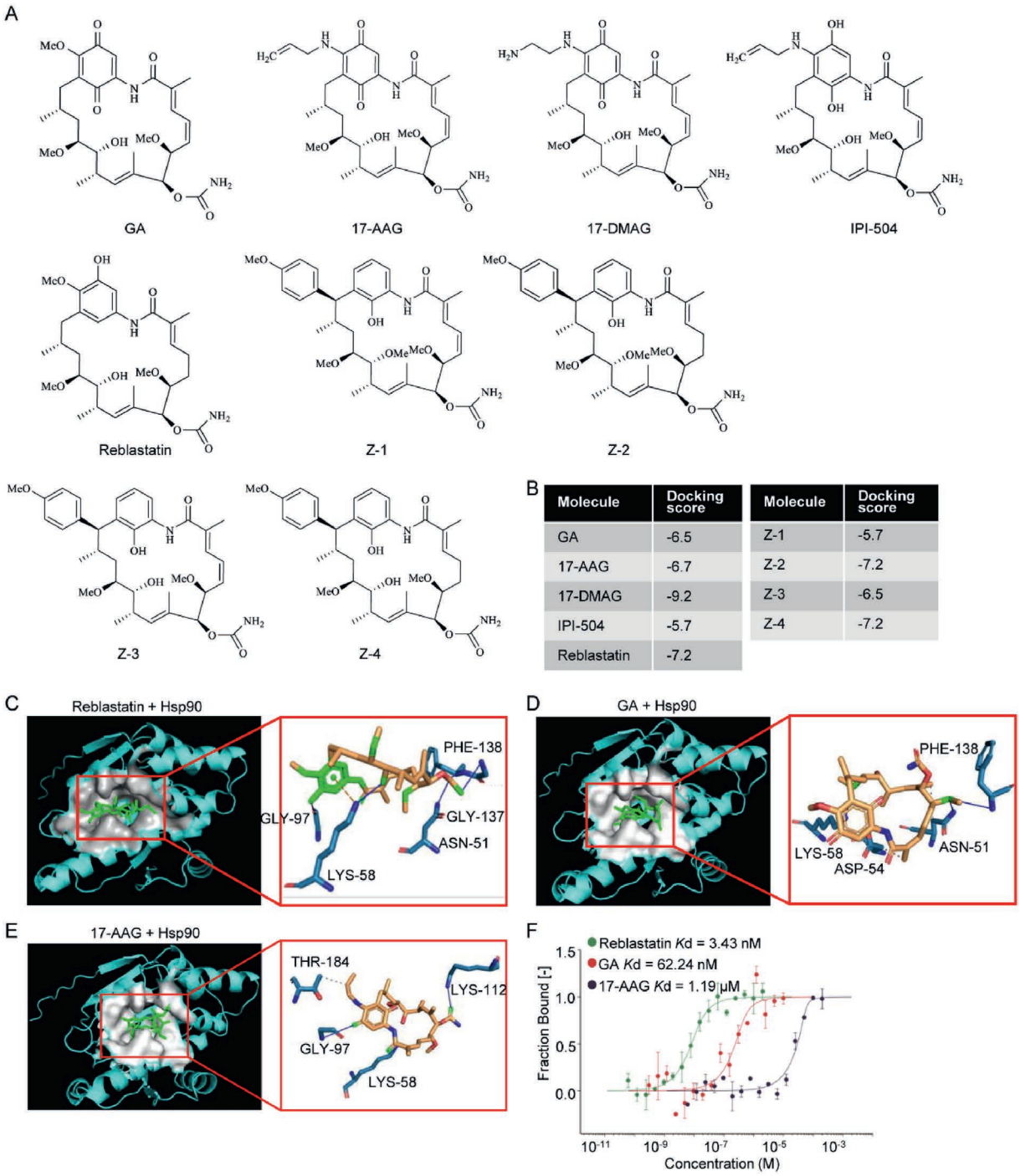

Molecule	Docking score	Molecule	Docking score
GA	-6.5	Z-1	-5.7
17-AAG	-6.7	Z-2	-7.2
17-DMAG	-9.2	Z-3	-6.5
IPI-504	-5.7	Z-4	-7.2
Reblastatin	-7.2		

Figure 1 Virtual screening and experimental verification of the binding affinities between benzenoid ansamycins and heat shock protein 90 (Hsp90). (A) Structures of 9 benzenoid ansamycin natural products and derivatives. (B) Binding energies of candidate compounds with Hsp90 (kJ/mol). (C−E) Binding conformation predictions between reblastatin and Hsp90, geldanamycin (GA) and Hsp90, or 17-AAG and Hsp90. (F) Binding curves of GA, 17-AAG, and reblastatin to Hsp90 in microscale thermophoresis assays. The K_D values are automatically generated by the MO Affinity analysis software ($n = 3$). Data are from three independent experiments. The results are presented as mean ± SEM. M, mol/L.

cell growth. In the HEK293 cell line, an immortalized human embryonic kidney cell line, the cytotoxicity of reblastatin was comparable to that of 17-AAG but significantly lower than that of GA after 48 and 72 h of treatment (Fig. 2A and B). In the HepG2 human liver carcinoma cell line, the IC_{50} values of reblastatin were 1.836 μmol/L and 1.477 μmol/L after 48 and 72 h of treatment, respectively, which were 5−20 times lower than those of GA and 17-AAG (Fig. 2C and D). In astrocytes, the IC_{50} values of reblastatin were 0.805 μmol/L and 0.760 μmol/L after 48 and 72 h of treatment, respectively, which were 8−20 times lower than those of GA and 17-AAG (Supporting Information Fig. S3A and S3B). Overall, the nonquinone benzenoid ansamycin reblastatin

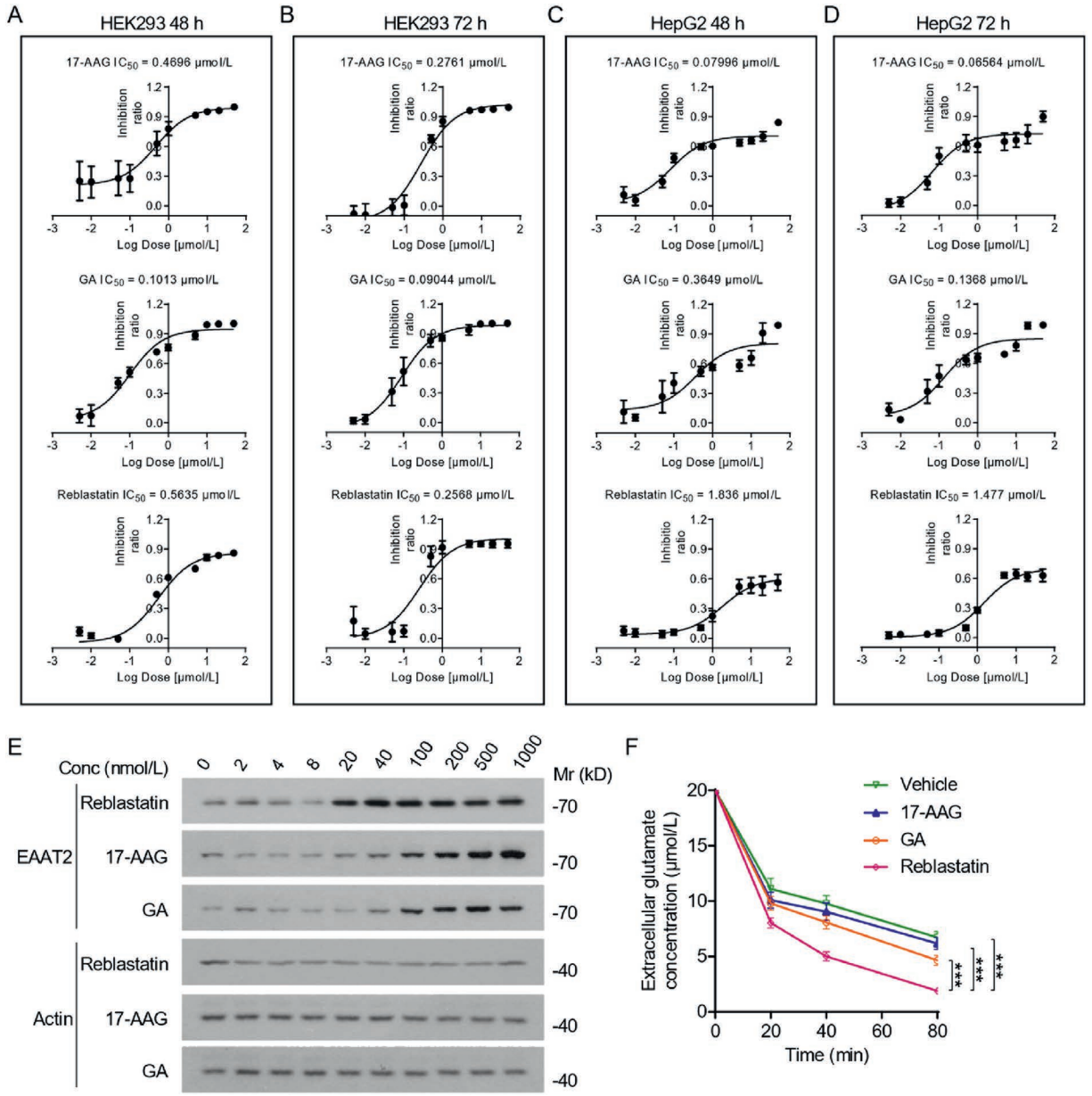

Figure 2 The cytotoxicity and glutamate uptake assay of reblastatin. (A−D) Cytotoxicity assays for 17-AAG, GA, and reblastatin in HEK293 and HepG2 cells ($n = 4$, nonlinear regression, dose-response-inhibition). (E) Western blotting analysis of excitatory amino acid transporter 2 (EAAT2) protein levels in primary cultured astrocytes treated for 24 h with GA, 17-AAG, or reblastatin at the indicated concentrations. (F) Extracellular glutamate uptake in primary cultured astrocytes following 36-h treatment with vehicle, GA (100 nmol/L), 17-AAG (100 nmol/L), or reblastatin (100 nmol/L), measured at various time points after incubation in the uptake buffer ($n = 3$ for each group, $^{***}P < 0.001$, one-way ANOVA with *post hoc* Tukey's multiple comparisons test). The results are presented as mean ± SEM.

exhibited markedly lower cytotoxicity compared to the other benzenoid ansamycins tested.

3.2. *Reblastatin promotes glutamate uptake by astrocytes*

Our previous study demonstrated that 17-AAG treatment increases EAAT2 protein levels in primary cultured astrocytes in a dose-dependent manner. Consistent with the binding affinity results, treatment with reblastatin at a concentration as low as 20 nmol/L for 48 h significantly elevated EAAT2 protein levels. In contrast, achieving the same effect with GA and 17-AAG required concentrations of 100−200 nmol/L (Fig. 2E). Moreover, reblastatin treatment enhanced glutamate uptake in primary cultured astrocytes, an effect not observed in the groups treated with GA and 17-AAG at the same dose (Fig. 2F). These findings suggest that low-dose systemic administration of reblastatin may offer a safer strategy for achieving effective Hsp90 inhibition in the brain.

3.3. *Pharmacokinetic profiles of reblastatin*

To evaluate the clinical potential of reblastatin, we examined its plasma protein binding, plasma stability, metabolism, and

pharmacokinetic profile (Supporting Information Fig. S4). Plasma protein binding was assessed using human, dog, rat, and mouse plasma (Fig. S4A), with warfarin and acetaminophen serving as controls for strong and weak plasma protein binding, respectively. The results indicated that reblastatin exhibits acceptable plasma protein binding rates across different species. The elimination half-life of reblastatin in rat and mouse plasma was 83.9 min and 113 min, respectively. In contrast, reblastatin showed minimal metabolism in human and dog plasma over 120 min, suggesting that it is stable in these species (Fig. S4B and S4C). Additionally, liver microsomal stability assays revealed that the elimination half-life of reblastatin was longer than that of midazolam in the liver microsomes of all four species tested. Specifically, the half-life was 18.4 min in humans, 17.9 min in dogs, 9.06 min in rats, and 9.43 min in mice (Fig. S4D and S4E).

Pharmacokinetic profiles of reblastatin were evaluated in CD-1 mice and SD rats following i.p., i.v., and intragastric (i.g.) administration (Supporting Information Fig. S5). In mice, 4 mg/kg reblastatin displayed rapid systemic absorption following i.p. administration, with a T_{max} of 0.25 h, a C_{max} of 838 ng/mL, and an AUC_{0-inf} of 805 ng h/mL. In contrast, after 10 mg/kg i.g. administration, systemic exposure was significantly reduced, with a C_{max} of only 4.42 ng/mL, an AUC_{0-t} of 20.0 ng h/mL, and a prolonged mean residence time (MRT_{0-t}) of 5.38 h. Intravenous administration at 2 mg/kg yielded an AUC_{0-inf} of 273.55 ng h/mL, a half-life ($t_{1/2}$) of 2.32 h, and an MRT_{0-inf} of 1.09 h (Fig. S5A−S5D). In SD rats, a similar trend was observed. After 4 mg/kg i.p. dosing, reblastatin showed a C_{max} of 1411.47 ng/mL and an AUC_{0-inf} of 1299.17 ng h/mL. Oral administration at 10 mg/kg resulted in a much lower C_{max} of 5.02 ng/mL and an AUC_{0-t} of 31.8 ng h/mL, with a notably delayed T_{max} of 3.67 h and prolonged MRT. Following 2 mg/kg i.v. administration, reblastatin exhibited a half-life of 2.75 h and an AUC_{0-inf} of 813 ng h/mL (Fig. S5E−S5H). Taken together, these results demonstrate that reblastatin exhibits favorable pharmacokinetic properties following parenteral administration. However, it displays poor oral bioavailability and undergoes rapid metabolic clearance.

To further investigate the time-dependent efficacy of reblastatin, an additional cohort of 12 mice was i.p. administered a single dose of 4 mg/kg reblastatin. Hippocampal EAAT2 levels were subsequently quantified at 0-, 24-, 48-, and 72-h post-dosing. As shown in Fig. S5I, hippocampal EAAT2 content peaked at the 48-h time point after a single dose administration. These data indicate that despite the rapid pharmacokinetic clearance observed in earlier analyses, reblastatin-mediated enhancement of EAAT2 protein level was sustained for up to 48−72 h.

3.4. Reblastatin increases hippocampal EAAT2 levels and inhibits seizures

To elucidate the molecular basis underlying Hsp90-mediated EAAT2 downregulation, we performed mechanistic investigations. EAAT2 exhibited reduced protein levels upon CHX administration. This CHX-induced EAAT2 reduction was attenuated by co-treatment with reblastatin, suggesting that reblastatin increased the protein stability of EAAT2 (Fig. 3A). Our previous study demonstrated physical interactions between Hsp90 and the 20S proteasome complex[30]. Co-immunoprecipitation experiments revealed the presence of a 20S proteasomal subunit within the EAAT2-Hsp90 protein complex. Importantly, reblastatin treatment disrupted not only the EAAT2-Hsp90 interaction but also the association between EAAT2 and the 20S proteasome (Fig. 3B). These findings collectively support a model wherein Hsp90 facilitates EAAT2 degradation by mediating its recruitment to the 20S proteasomal machinery, which is in line with our previous model deciphering Hsp90 inhibitor prevents GLT-1 degradation by disrupting the association between Hsp90, EAAT2 and 20S proteasome[30].

To evaluate the effects of reblastatin *in vivo*, the compound was administered to both normal mice and KA-induced chronic TLE model mice *via* i.p. injection 3 times over the course of a week. The hippocampi were then dissected for Western blotting analysis. As shown in Supporting Information Fig. S6A, reblastatin treatment at 2 mg/kg effectively increased EAAT2 levels in the hippocampi of normal mice.

In epileptic mice (Fig. 3C), we observed that i.p. injection of reblastatin at doses ranging from 1 to 4 mg/kg effectively increased hippocampal EAAT2 protein levels to a similar extent. However, administration of reblastatin at 10 mg/kg, a dose effective in normal mice, did not alter EAAT2 protein levels in the epileptic mice. This discrepancy is likely attributable to blood−brain barrier (BBB) disruption in epileptic mice[31-33], leading to more reblastatin entry into the brain and inhibiting *Slc1a2* transcription as reported in previous studies. First, administration of Evans blue demonstrated that the blood-brain barrier (BBB) was disrupted in the sclerotic hippocampus of TLE mice (Fig. S6B). Pharmacokinetic analysis of the hippocampus following a 4 mg/kg i.p. injection confirmed that reblastatin crossed the BBB and entered brain tissue more readily in epileptic mice than in normal mice (Fig. S6C and S6D). Secondly, as shown in Fig. S6E and S6F, the high dose (10 mg/kg) suppressed *Slc1a2* transcription by 50% in normal mice and 75% in epileptic mice. The effect of this Hsp90 inhibitor on EAAT2 protein levels represents a net balance between the inhibition of protein degradation and the suppression of gene transcription. The resulting inverted U-shaped dose-response curve indicates that the dosage of reblastatin must be controlled within a specific range, rather than assuming higher doses are more effective.

We next investigated whether reblastatin could reduce the number of spontaneous seizures in a mouse model of epilepsy. In PTZ-induced acute epilepsy model mice, we found that, compared to the control group and other dose treatment group, mice pretreated with reblastatin (4 mg/kg) had a lower Racine score (Fig. 3D) and a delayed seizure onset time (Fig. 3E). The 4 mg/kg and 10 mg/kg dose groups exhibited comparable therapeutic effects, both demonstrating significantly superior outcomes compared to the 1 and 2 mg/kg treatment groups. Based on integrated analysis of PTZ seizure tests and Western blotting results, the 4 mg/kg dose was selected for subsequent experiments. TLE was induced by intrahippocampal administration of KA, and reblastatin was administered at a dose of 4 mg/kg. This treatment significantly suppressed chronic epileptic seizures (Fig. 3H), reducing the number of seizures by 50% compared to baseline. In contrast, seizure frequency in the vehicle-treated group increased to 1.8-fold (Fig. 3F and G), which is consistent with reported results that seizures can increase in patients with TLE without clinical intervention[34].

To further evaluate the effects of reblastatin (4 mg/kg) on cognition and emotion in epileptic mice, we conducted two behavioral tests (open-field test and Y-maze test) in KA-induced chronic TLE mice. After 4 weeks of KA-induced epilepsy modeling, reblastatin was administered i.p. every other day for 2 weeks. As shown in Fig. 3I and J, the open-field test revealed a

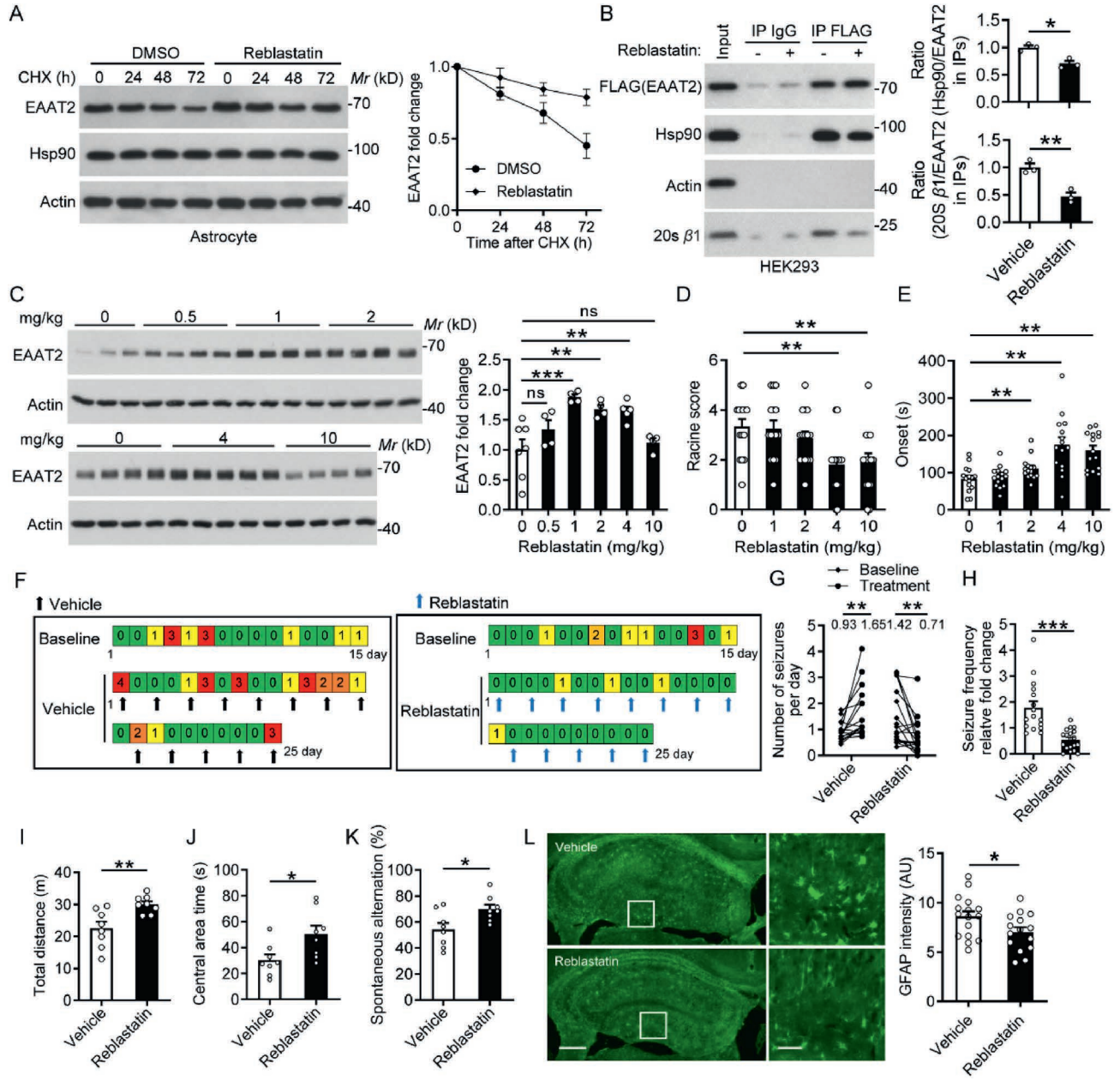

Figure 3 Reblastatin treatment inhibits spontaneous seizures and ameliorates reactive astrogliosis. (A) Western blotting of astrocytes treated with DMSO or reblastatin (100 nmol/L) in the presence of cycloheximide (CHX, 50 μg/mL) before harvesting (left). The line graph shows the relative fold change of EAAT2 (right, $n = 3$, normalized to actin). (B) Western blotting analysis for Hsp90-myc after immunoprecipitation of EAAT2-FLAG. HEK293 cells were cotransfected with Hsp90-myc and EAAT2-FLAG. 6 h after transfection, the cells were treated with or without reblastatin for 42 h (right, $n = 3$, normalized to actin, $^{*}P < 0.05$, $^{**}P < 0.01$, Student's *t*-test). (C) Western blotting of EAAT2 protein levels in the hippocampus of epileptic mice treated with vehicle or reblastatin (left). Reblastatin or vehicle was i.p. injected three times over the course of a week. The bar graph shows the relative fold change of EAAT2 (right, normalized to actin, $n = 3$, $^{**}P < 0.01$, $^{***}P < 0.001$, one-way ANOVA with Dunnett's *post hoc* test). (D−E) Assessments of reblastatin's effects in a pentetrazol (PTZ)-induced acute seizure model. Reblastatin was intraperitoneal (i.p.) injected once a day for three consecutive days; subsequently, the Racine score (D, $n = 15$ for each group, $^{**}P < 0.01$, Mann−Whitney U test) and onset time (E, $n = 15$ for each group, $^{**}P < 0.01$, Student's *t*-test) were assessed in response to acute PTZ injections (55 mg/kg). (F) Example seizure recordings following i.p. injection of reblastatin (4 mg/kg) or vehicle every other day. (G) Statistical analysis of seizures per day of epileptic mice treated with 4 mg/kg reblastatin ($n = 19$) or vehicle ($n = 16$) ($^{**}P < 0.01$, paired *t*-test). (H) Seizure frequency fold change of 4 mg/kg reblastatin or vehicle-treated epileptic mice (normalized to baseline, $^{***}P < 0.001$, Student's *t*-test). (I) Total distance traveled in the open field test by the mice treated with reblastatin ($n = 8$) and vehicle ($n = 8$) ($^{**}P < 0.01$, Student's *t*-test). (J) Time traveled in the central area in the open field test by the mice treated with reblastatin ($n = 8$) and vehicle ($n = 8$) ($^{*}P < 0.05$, Student's *t*-test). (K) Spontaneous alternations of mice treated with reblastatin ($n = 8$) and vehicle ($n = 8$) ($^{*}P < 0.05$, Student's *t*-test). (L) Immunofluorescence of glial fibrillary acidic protein (GFAP, left) and statistical analysis of GFAP intensity (right) in the sclerotic hippocampus of epileptic mice treated with 4 mg/kg reblastatin ($n = 16$) or vehicle ($n = 15$) (Left scale bar = 500 μm, Right scale bar = 100 μm, $^{*}P < 0.05$, Student's *t*-test). The results are presented as mean ± SEM. ns, not significant.

significant reduction in anxiety levels in drug-treated mice, accompanied by markedly increased total distance and prolonged central area time compared to controls. Similarly, the Y-maze results (Fig. 3K) demonstrated improved cognitive performance in the treated group compared to controls.

Given the bidirectional relationship between astrocyte reactiveness and seizure severity[35-37], we next evaluated GFAP immunofluorescence in the hippocampus ipsilateral to the KA injection. Reactive astrogliosis was significantly ameliorated in the reblastatin group compared to the control group (Fig. 3L). Furthermore, reblastatin-treated TLE mice showed reduced S100β levels and upregulation of glutamine synthetase (GS) in astrocytes relative to vehicle-treated mice (Supporting Information Fig. S7A−S7D), suggesting that reblastatin attenuates astrocyte-mediated inflammation and enhances astrocytic glutamate metabolic capacity, respectively. In addition, as a positive control, we observed that the TLE model mice treated with CBZ showed some therapeutic effects in the early stages but developed varying degrees of resistance to CBZ in the later stages (Fig. S7E and S7F), consistent with previous findings[25]. Together, these findings suggest that low-dose reblastatin exerts a significant antiseizure effect in mice with spontaneous epilepsy.

3.5. Reblastatin has therapeutic effects on PD and AD mice

Excitotoxicity is a hallmark pathological mechanism underlying many neurodegenerative diseases, including AD and PD[38]. Reducing glutamate levels in these diseases is considered a potential neuroprotective therapy. Although *N*-methyl-D-aspartate receptor (NMDAR) antagonists, most of which block the NMDAR channel, have been shown to exert anti-excitotoxicity effects in various mouse models, none are suitable for long-term use due to their severe side effects[39]. Given that reblastatin has demonstrated antiepileptic effects in mouse models of TLE, we next tested whether reblastatin offers therapeutic benefits in mouse models of PD and AD.

To evaluate the therapeutic effects of reblastatin on PD, we conducted behavioral assessments on the mice following drug administration (Fig. 4A). In the pole test, reblastatin-treated mice exhibited a significantly shorter time to descend the pole compared to the control group (Fig. 4B). The movement trajectories of mice in the open field test are shown in Fig. 4C. Quantitative analysis revealed that reblastatin administration significantly increased the total travel distance (Fig. 4D) and prolonged the time spent in the central area (Fig. 4E). Moreover, reblastatin improved the performance of mice in the wire hang test (Fig. 4F). The elevated plus maze test confirmed that reblastatin did not induce anxiety-like behaviors (Supporting Information Fig. S8A−S8D). Collectively, these findings demonstrate that reblastatin alleviates motor deficits in PD mice.

We selected three distinct sections of the mouse brain substantia nigra for immunofluorescence staining of TH. The progressive degeneration of dopaminergic (DA) neurons in the midbrain substantia nigra, along with a decrease in DA neurotransmitter levels in associated brain regions, constitutes the pathological basis for the development of PD. In humans, DA is synthesized from tyrosine, the primary substrate, with TH serving as the critical rate-limiting enzyme. The activity of TH directly influences the intracellular DA content in dopaminergic neurons. Immunofluorescence results indicated that following i.p. injection of reblastatin in the experimental group, the number of TH-positive neurons in the substantia nigra significantly increased compared to the control group (Fig. 4G), suggesting that reblastatin may play a protective role against MPTP-induced dopaminergic neurotoxicity in the substantia nigra.

The epileptic phenotype is frequently observed in APP mice[40]. APP/PS1 mice are an essential model for investigating the underlying mechanisms of AD-related epilepsy and evaluating potential therapeutic interventions. Western blotting analysis of hippocampal EAAT2 protein levels revealed an increase in EAAT2 protein level in the hippocampus of the experimental group compared to the control group (Fig. 5A). To more objectively evaluate seizures in mice, we analyzed the vEEG characteristics in APP/PS1 mice (Fig. 5B). The results indicated that after administration of 4 mg/kg reblastatin, APP/PS1 mice had less severe epileptiform activities compared with baseline period (Fig. 5C−F). Following vEEG monitoring, both groups of mice underwent a novel object recognition test. Results showed that mice in the reblastatin-treated group displayed a stronger exploratory preference for the novel object (Fig. 5G and H), indicating that reblastatin can alleviate cognitive impairment in AD mice. These findings suggest that reblastatin could reduce spontaneous epilepsy-like discharges in AD mice and exert a therapeutic effect on cognitive impairment.

The Morris water maze test was used to assess spatial learning and memory after reblastatin treatment. Six-month-old APP/PS1 mice were treated for 2.5 months with reblastatin, memantine (an NMDAR-targeting control drug), or vehicle. All groups successfully located the cued platform (Fig. S8E). During hidden-platform training, reblastatin ameliorated spatial learning deficits in AD mice, as reflected by a significant decrease in escape latency (Fig. S8F). In a probe trial performed 24 h after the last training session, reblastatin-treated AD mice spent significantly more time in the target quadrant than vehicle-treated AD mice (Fig. S8G). In contrast, memantine conferred no cognitive benefits in this paradigm, aligning with previous studies reporting its lack of significant effects on cognition in AD mouse models[41] or patients[42,43]. Furthermore, hippocampal cleaved caspase-3 staining revealed a marked reduction in apoptotic neurons in the reblastatin group compared to vehicle controls (Fig. S8H−S8K). Together, these data further support the neuroprotective potential of reblastatin.

3.6. In vivo toxicity of reblastatin

To assess the toxicity of reblastatin, we conducted toxicity tests in normal mice that received i.p. injections of vehicle, GA, 17-AAG, or reblastatin at 4 or 20 mg/kg. The treatments were administered every other day for a total of seven injections. All mice exhibited normal weight gain except for those treated with 20 mg/kg GA, which resulted in 100% mortality (Fig. 6A). Consequently, only the remaining six groups were analyzed. No significant differences in liver mass or liver coefficient were observed among these groups (Fig. 6B and C). HE staining revealed hepatic vacuolar changes in 100% of the mice treated with 4 mg/kg GA, 67% of those treated with 4 mg/kg 17-AAG, and 83% of those treated with 20 mg/kg 17-AAG. In contrast, only 29% of the mice in the 4 and 20 mg/kg reblastatin groups exhibited liver injury, a percentage comparable to that of the control group (20%; Fig. 6D and E). Additionally, serum levels of AST, ALT, BUN, and CREA were measured in each group. The results indicated that mice treated with 4 mg/kg GA and 17-AAG had significantly higher serum AST levels compared to the other groups (Fig. 6F), although ALT levels did not differ significantly among the groups

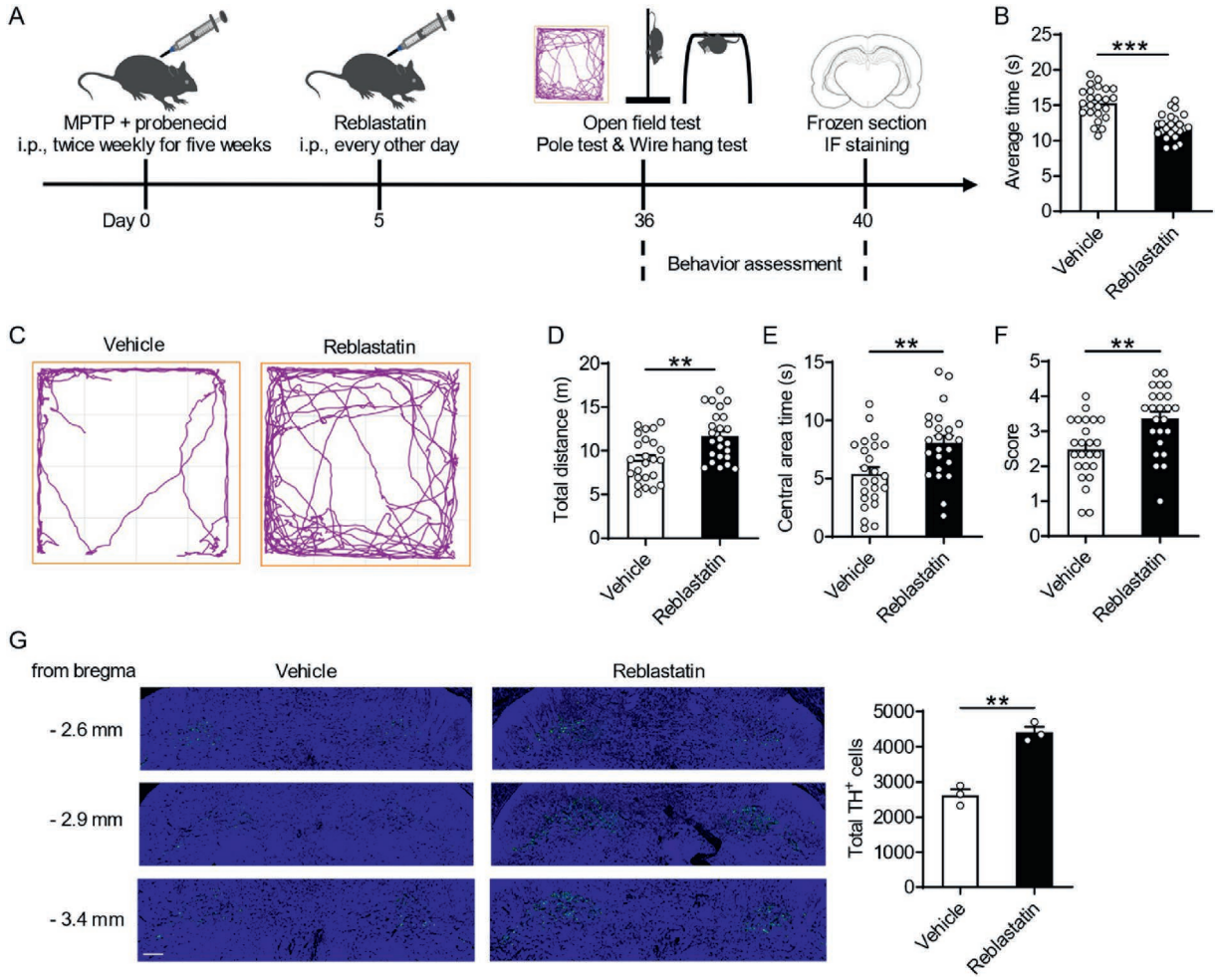

Figure 4 Reblastatin has a therapeutic effect on Parkinson's disease (PD) mice. (A) Experimental design of the study and behavior assessment on PD mice. (B) Time taken to climb down in the pole test from mice treated with reblastatin ($n = 24$) and vehicle ($n = 24$) (***$P < 0.001$, Student's t-test). (C) Track map of mice in the open field. (D) Total distance traveled in the open field test by the mice treated with reblastatin ($n = 24$) and vehicle ($n = 24$) (**$P < 0.01$, Student's t-test). (E) Time traveled in the central area in the open field test by the mice treated with reblastatin ($n = 24$) and vehicle ($n = 24$) (**$P < 0.01$, Student's t-test). (F) Wire hang test scores of mice treated with reblastatin ($n = 24$) and vehicle ($n = 24$) (**$P < 0.01$, Student's t-test). (G) Immunofluorescence of tyrosine hydroxylase (TH, left) and statistical analysis of the number of TH-positive neurons (right) in the substantia nigra of PD mice treated with vehicle ($n = 3$) and 4 mg/kg reblastatin ($n = 3$) (Scale bar = 300 μm, **$P < 0.01$, Student's t-test). The results are presented as mean ± SEM.

(Fig. 6G). The AST/ALT ratio analysis suggested that GA was the most toxic Hsp90 inhibitor among these chemicals (Fig. 6H). No significant differences in serum BUN or CREA levels were observed across the treatment groups (Fig. 6I and J). Based on these findings, we conclude that the toxicity of reblastatin at both 4 mg/kg and 20 mg/kg is relatively mild and nearly indistinguishable from that of the vehicle control.

To evaluate potential long-term toxicity and multiorgan effects, we performed a three-month chronic administration study of reblastatin (4 mg/kg) and memantine (10 mg/kg). Serum biochemical analysis showed no significant differences in any of the 15 hematological parameters among reblastatin-, memantine-, and vehicle-treated groups (Supporting Information Fig. S9A−S9O). Consistent with serum biochemistry findings, histopathological evaluation of liver and kidney sections showed unremarkable morphology across all treatment groups (Fig. S9P). Hepatic structure was intact, and renal assessment revealed well-preserved glomeruli and tubules with no evidence of degeneration, necrosis, or inflammatory infiltration. Taken together, these data confirm the absence of notable histotoxicity following prolonged reblastatin exposure.

Additionally, proteomic analysis of hippocampal tissues from reblastatin-treated mice compared to vehicle-treated controls identified a total of 6660 proteins, among which 54 were significantly downregulated, and 14 were upregulated. Gene Ontology (GO) enrichment analysis of these differentially expressed proteins revealed no enrichment of overlapping pathways (Supporting Information Table S2). These findings suggest that reblastatin administration at the therapeutic dose does not induce widespread off-target effects at the proteome level, and the observed proteomic changes are not associated with known epileptogenic mechanisms.

4. Discussion

Reblastatin is a phenolic analog of GA with Hsp90 inhibitory and antiproliferative activity. Like GA, reblastatin binds to the

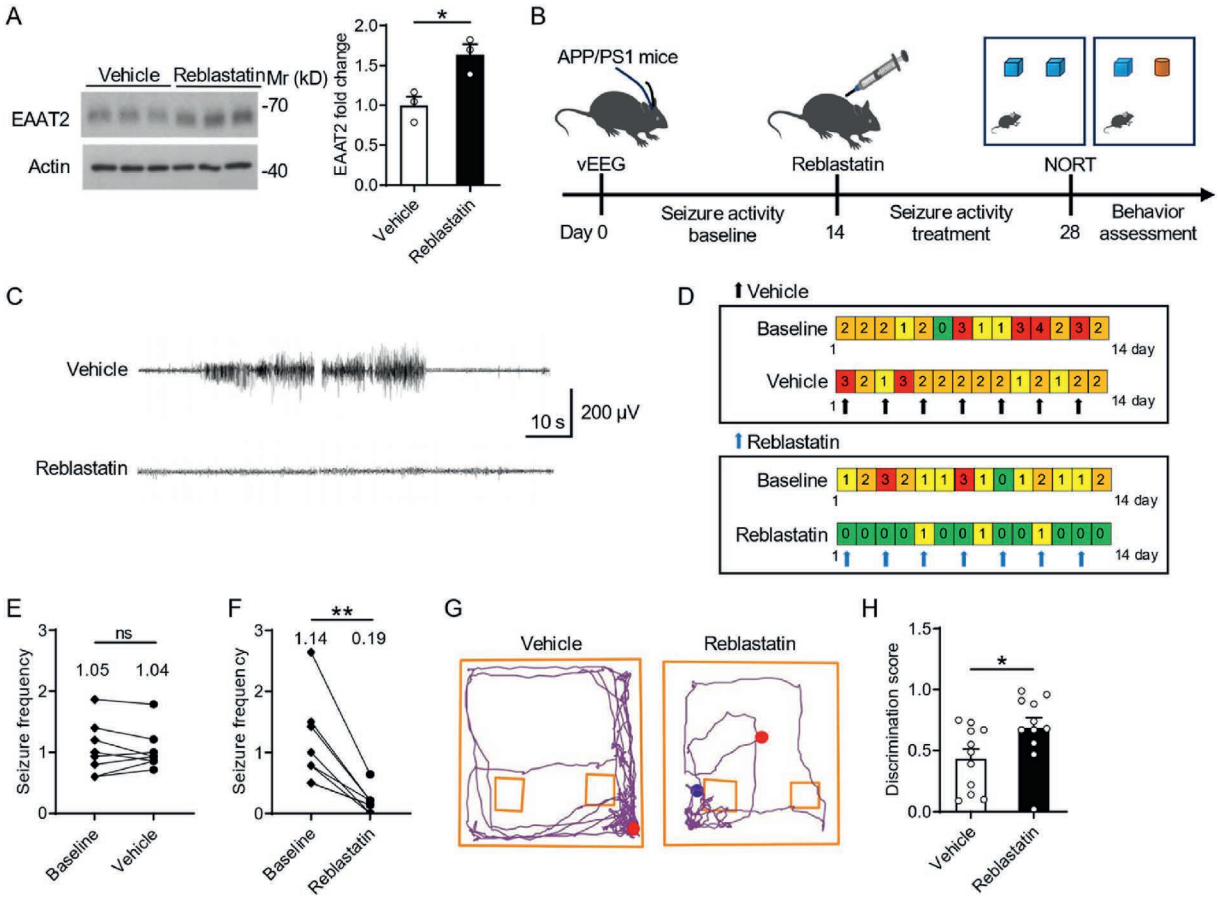

Figure 5 Reblastatin has a therapeutic effect on Alzheimer's disease (AD) mice. (A) Western blotting of EAAT2 protein levels in the hippocampus of *Appswe/Ps1dE9* transgenic (APP/PS1) mice received i.p. injection of vehicle or 4 mg/kg reblastatin every other day for 3 total injections (left). The bar graph shows the relative fold change of EAAT2 (right, normalized to actin, $n = 3$, $^{*}P < 0.05$, Student's *t*-test). (B) Experimental design of the study and behavioral test on AD mice, reblastatin (4 mg/kg) or vehicle was i.p. injected every other day. (C) Examples of electroencephalogram tracings from a vehicle-treated subject (upper) and a subject treated with reblastatin (4 mg/kg, lower). (D) Examples of seizures recorded from mice treated with 4 mg/kg reblastatin or vehicle. (E, F) Statistical analysis of seizures per day of APP/PS1 mice treated with vehicle (E, $n = 8$) or 4 mg/kg reblastatin (F, $n = 8$, $^{**}P < 0.01$, paired *t* test). (G) Track map of mice in the novel object recognition test. (H) Discrimination score of APP/PS1 mice treated with 4 mg/kg reblastatin ($n = 11$) and vehicle ($n = 11$) ($P < 0.05$, Student's *t*-test). Discrimination score = new object exploration time/total exploration time. The results are presented as mean ± SEM. ns, not significant.

N-terminal ATP-binding site of Hsp90, blocking ATP binding and thereby inhibiting Hsp90 function[20,44]. Nonquinone derivatives, such as reblastatin, exhibit stronger Hsp90 inhibition compared to GA, which contains a benzoquinone structure[45]. Guo et al.[46] demonstrated that reducing the benzoquinone structure of 17-AAG to a hydroquinone structure enhances its Hsp90 inhibition and increases its stability within cells. The reduced form of 17-AAG shows higher affinity for Hsp90 and a slower dissociation rate than its oxidized form[47]. By blocking the Hsp90-mediated 20S proteasomal degradation pathway of EAAT2, reblastatin effectively prevents EAAT2 degradation in astrocytes and promotes extracellular glutamate uptake.

In our study, we compared the affinities of reblastatin, GA, and 17-AAG for Hsp90 using MST and molecular docking. The results showed that reblastatin had the highest affinity for Hsp90. Furthermore, primary cultured astrocytes treated with reblastatin exhibited the highest levels of extracellular glutamate uptake. Our previous research identified an effective antiepileptic dose of 25 mg/kg for 17-AAG in mice[15], whereas the current study demonstrated that a significantly lower dose of 4 mg/kg reblastatin is sufficient to achieve an anti-excitotoxic effect. The IC_{50} of reblastatin was significantly higher than that of GA and 17-AAG in HEK293 and HepG2 cells following long-term treatment, indicating lower cytotoxicity. In the acute toxicity assay, reblastatin-treated mice exhibited phenotypes nearly identical to those of vehicle-treated mice. In contrast, mice treated with GA and 17-AAG displayed varying degrees of liver injury. Moreover, the multi-organ toxicity data demonstrate that reblastatin exhibits a favorable safety profile in both short- and long-term dosing regimens. While minor biochemical fluctuations and non-specific histological alterations were observed, these changes were not associated with overt functional impairment or structural damage in hepatic, renal, or cardiac tissues. Collectively, these findings provide preliminary evidence supporting the therapeutic potential of reblastatin.

In a previous study, the IC_{50} values of GA and reblastatin were found to be 0.0011 and 0.43 μg/mL, respectively, in human histiocytic lymphoma U-937 cells. The XTT assay revealed that reblastatin primarily inhibited the cell cycle rather than inducing apoptosis, suggesting that its inherent cytotoxicity is extremely

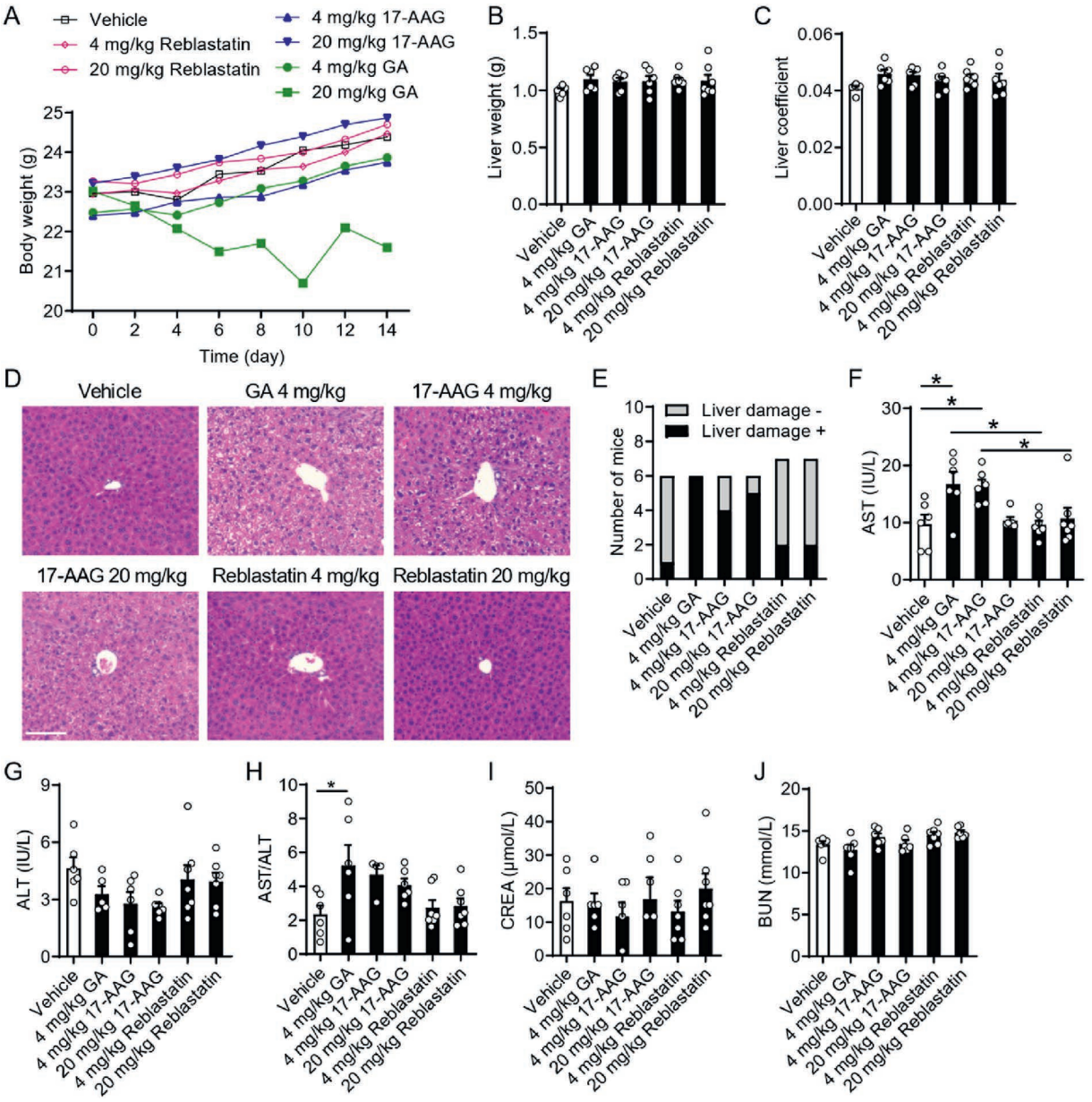

Figure 6 Reblastatin shows no obvious acute toxicity. (A) Body weight changes with time. Mice were i.p. injected with 4 mg/kg GA, 4 mg/kg 17-AAG, 20 mg/kg 17-AAG, 4 mg/kg reblastatin, or 20 mg/kg reblastatin once every other day for 2 weeks. (B, C) Statistical analysis of liver weight and liver coefficient of mice under acute toxicity test ($n = 6$). (D) Hematoxylin−eosin (HE) staining of liver paraffin sections from acute toxicity-treated mice (Scale bar = 200 μm). (E) Statistics of liver damage in acute toxicity-treated mice. (F−J) Serum aminotransferase (AST), alanine aminotransferase (ALT), AST/ALT, creatinine (CREA), blood urea nitrogen (BUN) of mice in acute toxicity treatment groups ($n = 6$, $^*P < 0.05$, one-way ANOVA with post-hoc Tukey's multiple comparisons test). The results are presented as mean ± SEM.

low[48]. The toxicity of GA is largely attributed to its benzoquinone structure, which leads to reactive oxygen species generation through redox cycling and alkylation of cellular nucleophilic groups[49]. Additionally, the quinone group can interact with the two-electron reductase NQO1, further disrupting normal cellular functions[50]. A previous *in vitro* assay demonstrated that the EC_{50} of reblastatin for Hsp90 is 10 times lower than that of GA[51]. Moreover, replacing the *para*-benzoquinone moiety with a phenol ring can significantly reduce or even eliminate the hepatotoxic effects associated with the benzoquinone group, while maintaining the overall topology of the ansamycin framework and its binding affinity for Hsp90[52].

Reactive astrocytes and epileptic seizures influence each other in a reinforcing cycle: seizures rapidly activate microglia, which release inflammatory signals that sustain astrocyte reactivity[53]; in turn, reactive astrocytes enhance neuronal hyperexcitability and promote further seizures[54]. These findings support the view that reactive astrocytes play central roles in both the onset and progression of epilepsy, suggesting that targeting astrocyte activity could offer therapeutic benefit[55], especially in TLE. In our study, reblastatin treatment was associated with reduced astrocyte reactivity. While Hsp90 inhibitors have not been shown to directly inhibit astrocytes, we propose this reduction may be an indirect effect resulting from seizure suppression.

Reblastatin exhibits an inverted U-shaped dose-response relationship for EAAT2 induction in epileptic mice. While doses of 1−4 mg/kg effectively increased hippocampal EAAT2 protein levels, the 10 mg/kg dose—which is effective in normal mice—failed to do so in the epileptic group. This loss of efficacy is likely due to 2 factors: suppression of *Slc1a2* transcription at higher doses (75% reduction in epileptic mice *vs.* 50% in normal mice), and increased penetration of reblastatin across the compromised BBB in TLE, as supported by pharmacokinetic evidence. Notably, this biphasic response is not unique to reblastatin but was also observed with two other structurally distinct Hsp90 inhibitors[15,56], suggesting that the dosage of reblastatin must be controlled within a specific range, rather than assuming higher doses are more effective.

Pharmacokinetic analysis revealed that reblastatin exhibits excellent stability in plasma, particularly in human plasma, where it is not metabolized. Its moderate binding to plasma proteins enables efficient transport to target tissues and organs. However, the comprehensive pharmacokinetic evaluation of reblastatin through hepatic microsomal metabolism assays and rodent pharmacokinetic studies revealed several critical limitations that necessitate further structural optimization. Our data demonstrated rapid metabolic clearance of reblastatin in both murine and rat models, accompanied by significantly reduced brain tissue concentrations relative to plasma levels, indicative of poor blood-brain barrier penetration. Furthermore, comparative oral *versus* intravenous administration studies established the compound's low oral bioavailability. These findings collectively underscore the need for systematic structural modifications to address the metabolic instability, enhance central nervous system delivery, and improve oral absorption characteristics of reblastatin. Moving forward, we will focus on rational drug design approaches to develop optimized derivatives, followed by thorough preclinical characterization of their pharmacological properties. The most promising candidates will then be advanced through rigorous preclinical development with the ultimate goal of identifying a clinically viable therapeutic agent. This iterative optimization and evaluation strategy aims to transform reblastatin's pharmacological profile while maintaining its therapeutic potential.

Critically, the pathophysiological mechanisms underlying TLE—such as neuroinflammation[57], synaptic dysfunction, and excitotoxicity—share striking similarities with those driving neurodegenerative diseases like PD and AD. Although reblastatin was initially developed specifically for TLE, its mechanism of action indicates potential for broader applications, particularly in the treatment of excitotoxicity-related diseases. This dual focus reflects the hypothesis that targeting shared pathological mechanisms may yield translational benefits across distinct neurological conditions. The concentration of glutamate in the synaptic cleft is tightly regulated by the balance between its release and clearance. Excessive glutamate overstimulates glutamate receptors, leading to elevated intracellular concentrations of sodium and calcium ions, which can directly cause neuronal damage and cell death. High glutamate levels can also activate glial cells and exacerbate the imbalance in glutamate metabolism[58]. Currently, there are no safe and effective drugs available to prevent excitotoxicity. Given that excessive NMDAR activation plays a key role in glutamate excitotoxicity, blocking these receptors has been explored as a potential therapeutic strategy[59]. However, most NMDAR antagonists are competitive, and they tend to interfere with normal brain function, often resulting in significant side effects[60]. An alternative approach to prevent excitotoxicity involves enhancing astrocyte-mediated glutamate reuptake. Mice lacking the EAAT2 transporter exhibit spontaneous lethal seizures and heightened sensitivity to acute cortical injury[61], suggesting that upregulating EAAT2 may provide a promising strategy for mitigating excitotoxicity.

In PD models, the expression of EAAT2 has been a focus of investigation. Downregulation of EAAT2 has been reported in both 6-hydroxydopamine-induced and acute MPTP-induced PD models, particularly in the mouse striatum[62,63]. These findings highlight the critical role of EAAT2 regulation in maintaining glutamate homeostasis and suggest that targeting EAAT2 could offer therapeutic potential for excitotoxicity-related diseases. Our research using an MPTP-induced PD mouse model has confirmed that reblastatin can alleviate the motor symptoms of PD, probably by addressing underlying neurochemical imbalances. These findings open a promising avenue for treating PD.

Approximately 10%−22% of AD patients are estimated to experience unprovoked seizures. Spontaneous seizures and spike-wave discharges have also been documented in AD-related animal models. In the widely used APP/PS1 mouse model, a reduction in EAAT2 levels within the hippocampus has been observed[64]. Our study demonstrates that reblastatin significantly reduces the frequency and severity of spontaneous epileptic discharges in APP/PS1 mice, suggesting its potential therapeutic value. Previous research found that cognitive function improved in APP/PS1 mice following treatment with an EAAT2 translational activator[65]. However, the etiology of epilepsy in AD is complex, with multiple contributing factors[66]. Future research should therefore take into account the interplay of these various factors when exploring therapeutic strategies.

Our current research is dedicated to evaluating the translational potential of novel therapeutic compounds, with particular emphasis on the optimization of their oral formulations during the preclinical development stage. To further support this translational effort, future studies may benefit from the incorporation of human-derived epileptic brain organoid models, which offer a physiologically relevant platform to assess therapeutic efficacy in a context that more closely recapitulates the complex cellular and network dynamics of the human brain. In parallel, advanced *in vitro* blood-brain barrier models should be employed to enable systematic pharmacokinetic characterization of cerebral penetration, which remains a critical determinant of central nervous system (CNS) drug delivery. Collectively, these complementary approaches are expected to yield mechanistically informative and clinically relevant data regarding both CNS bioavailability and therapeutic action, thereby providing a stronger empirical foundation for the rational progression of candidate compounds toward clinical evaluation.

5. Conclusions

In this study, we demonstrated that the Hsp90 inhibitor reblastatin effectively increases EAAT2 levels in the epileptogenic focus. Reblastatin reduced seizure frequency in both PTZ- and KA-induced TLE mouse models and exhibited robust therapeutic effects in models of PD and AD. As a non-benzoquinone ansamycin, reblastatin showed superior Hsp90 binding affinity, lower toxicity, and reduced treatment dose requirements compared to current benzoquinone ansamycin Hsp90 inhibitors. These attributes position reblastatin as a promising candidate for further development as an antiepileptic drug and a neuroprotective agent

against excitotoxicity-related diseases. Optimizing its structure and delivery will be crucial to enabling successful clinical translation.

Acknowledgments

This work was supported by research grants from the National Natural Science Foundation of China (82571662, 82171447, and 32293213) and the CAMS Innovation Fund for Medical Sciences (2021-I2M-1-020, China).

Author contributions

Xiuneng Zhang: investigation, formal analysis, validation, writing - original draft preparation. Xiaolin Yu: investigation, formal analysis, writing - original draft preparation. Longze Sha: conceptualization, investigation, writing - reviewing and editing, project administration. Yunfeng Li: investigation. Qi Qiao: investigation. Xiaoming Yu: conceptualization, resources. Qi Xu: conceptualization, resources, project administration.

Conflicts of interest

The authors declare no conflicts of interest.

Appendix A. Supporting information

Supporting information to this article can be found online at https://doi.org/10.1016/j.apsb.2026.02.017.

References

1. World Health Organization. Epilepsy: a public health imperative. 2019-06-20. Available from: https://iris.who.int/items/e74f31ae-9646-49ba-8b0b-50430f597609/full.
2. Chen Z, Brodie MJ, Liew D, Kwan P. Treatment outcomes in patients with newly diagnosed epilepsy treated with established and new antiepileptic drugs: a 30-year longitudinal cohort study. *JAMA Neurol* 2018;**75**:279−86.
3. Kwan P, Brodie MJ. Early identification of refractory epilepsy. *N Engl J Med* 2000;**342**:314−9.
4. Fattorusso A, Matricardi S, Mencaroni E, Dell'Isola GB, Di Cara G, Striano P, et al. The pharmacoresistant epilepsy: an overview on existent and new emerging therapies. *Front Neurol* 2021;**12**:674483.
5. Danbolt NC. Glutamate uptake. *Prog Neurobiol* 2001;**65**:1−105.
6. Souza DG, Almeida RF, Souza DO, Zimmer ER. The astrocyte biochemistry. *Semin Cell Dev Biol* 2019;**95**:142−50.
7. Ammothumkandy A, Ravina K, Wolseley V, Tartt AN, Yu PN, Corona L, et al. Altered adult neurogenesis and gliogenesis in patients with mesial temporal lobe epilepsy. *Nat Neurosci* 2022;**25**:493−503.
8. Holmseth S, Scott HA, Real K, Lehre KP, Leergaard TB, Bjaalie JG, et al. The concentrations and distributions of three C-terminal variants of the GLT1 (EAAT2; slc1a2) glutamate transporter protein in rat brain tissue suggest differential regulation. *Neuroscience* 2009;**162**:1055−71.
9. Mathern GW, Mendoza D, Lozada A, Pretorius JK, Dehnes Y, Danbolt NC, et al. Hippocampal GABA and glutamate transporter immunoreactivity in patients with temporal lobe epilepsy. *Neurology* 1999;**52**:453−72.
10. Poletti S, Bollettini I, Lorenzi C, Vitali A, Brioschi S, Serretti A, et al. White matter microstructure in bipolar disorder is influenced by the interaction between a glutamate transporter *EAAT1* gene variant and early stress. *Mol Neurobiol* 2019;**56**:702−10.
11. Garcia-Esparcia P, Diaz-Lucena D, Ainciburu M, Torrejón-Escribano B, Carmona M, Llorens F, et al. Glutamate transporter GLT1 expression in Alzheimer disease and dementia with Lewy bodies. *Front Aging Neurosci* 2018;**10**:122.
12. Sarac S, Afzal S, Broholm H, Madsen FF, Ploug T, Laursen H. Excitatory amino acid transporters EAAT-1 and EAAT-2 in temporal lobe and hippocampus in intractable temporal lobe epilepsy. *APMIS* 2009;**117**:291−301.
13. Iovino L, Giusti V, Pischedda F, Giusto E, Plotegher N, Marte A, et al. Trafficking of the glutamate transporter is impaired in LRRK2-related Parkinson's disease. *Acta Neuropathol* 2022;**144**:81−106.
14. Takasaki C, Okada R, Mitani A, Fukaya M, Yamasaki M, Fujihara Y, et al. Glutamate transporters regulate lesion-induced plasticity in the developing somatosensory cortex. *J Neurosci* 2008;**28**:4995−5006.
15. Sha L, Wang X, Li J, Shi X, Wu L, Shen Y, et al. Pharmacologic inhibition of Hsp90 to prevent GLT-1 degradation as an effective therapy for epilepsy. *J Exp Med* 2017;**214**:547−63.
16. Lin CL, Kong Q, Cuny GD, Glicksman MA. Glutamate transporter EAAT2: a new target for the treatment of neurodegenerative diseases. *Future Med Chem* 2012;**4**:1689−700.
17. Liew HY, Tan XY, Chan HH, Khaw KY, Ong YS. Natural HSP90 inhibitors as a potential therapeutic intervention in treating cancers: a comprehensive review. *Pharmacol Res* 2022;**181**:106260.
18. Samuni Y, Ishii H, Hyodo F, Samuni U, Krishna MC, Goldstein S, et al. Reactive oxygen species mediate hepatotoxicity induced by the Hsp90 inhibitor geldanamycin and its analogs. *Free Radic Biol Med* 2010;**48**:1559−63.
19. DeBoer C, Meulman PA, Wnuk RJ, Peterson DH. Geldanamycin, a new antibiotic. *J Antibiot (Tokyo)* 1970;**23**:442−7.
20. Schulte TW, Akinaga S, Soga S, Sullivan W, Stensgard B, Toft D, et al. Antibiotic radicicol binds to the N-terminal domain of Hsp90 and shares important biologic activities with geldanamycin. *Cell Stress Chaperones* 1998;**3**:100−8.
21. Supko JG, Hickman RL, Grever MR, Malspeis L. Preclinical pharmacologic evaluation of geldanamycin as an antitumor agent. *Cancer Chemother Pharmacol* 1995;**36**:305−15.
22. Talaei S, Mellatyar H, Asadi A, Akbarzadeh A, Sheervalilou R, Zarghami N. Spotlight on 17-AAG as an Hsp90 inhibitor for molecular targeted cancer treatment. *Chem Biol Drug Des* 2019;**93**:760−86.
23. Bisht KS, Bradbury CM, Mattson D, Kaushal A, Sowers A, Markovina S, et al. Geldanamycin and 17-allylamino-17-demethoxygeldanamycin potentiate the *in vitro* and *in vivo* radiation response of cervical tumor cells *via* the heat shock protein 90-mediated intracellular signaling and cytotoxicity. *Cancer Res* 2003;**63**:8984−95.
24. Miralles VJ, Martínez-López I, Zaragozá R, Borrás E, García C, Pallardó FV, et al. Na^+ dependent glutamate transporters (EAAT1, EAAT2, and EAAT3) in primary astrocyte cultures: effect of oxidative stress. *Brain Res* 2001;**922**:21−9.
25. Li J, Sha L, Xu Q. Long-term outcomes of classic and novel antiseizure medication in a kainate-induced model of chronic epilepsy. *Epilepsy Res* 2023;**191**:107095.
26. Lisgaras CP, Scharfman HE. Robust chronic convulsive seizures, high frequency oscillations, and human seizure onset patterns in an intrahippocampal kainic acid model in mice. *Neurobiol Dis* 2022;**166**:105637.
27. Williams PA, White AM, Clark S, Ferraro DJ, Swiercz W, Staley KJ, et al. Development of spontaneous recurrent seizures after kainate-induced status epilepticus. *J Neurosci* 2009;**29**:2103−12.
28. Shao QH, Chen Y, Li FF, Wang S, Zhang XL, Yuan YH, et al. TLR4 deficiency has a protective effect in the MPTP/probenecid mouse model of Parkinson's disease. *Acta Pharmacol Sin* 2019;**40**:1503−12.
29. Fu X, Zhou G, Wu X, Xu C, Zhou H, Zhuang J, et al. Inhibition of P2X4R attenuates white matter injury in mice after intracerebral hemorrhage by regulating microglial phenotypes. *J Neuroinflammation* 2021;**18**:184.
30. Eleuteri AM, Cuccioloni M, Bellesi J, Lupidi G, Fioretti E, Angeletti M. Interaction of Hsp90 with 20S proteasome: thermodynamic and kinetic characterization. *Proteins* 2002;**48**:169−77.

31. Sokrab TEO, Kalimo H, Johansson BB. Parenchymal changes related to plasma protein extravasation in experimental seizures. *Epilepsia* 1990;**31**:1−8.
32. Pont F, Collet A, Lallement G. Early and transient increase of rat hippocampal blood−brain barrier permeability to amino acids during kainic acid-induced seizures. *Neurosci Lett* 1995;**184**:52−4.
33. Lassmann H, Petsche U, Kitz K, Baran H, Sperk G, Seitelberger F, et al. The role of brain edema in epileptic brain damage induced by systemic kainic acid injection. *Neuroscience* 1984;**13**:691−704.
34. Coan AC, Cendes F. Epilepsy as progressive disorders: what is the evidence that can guide our clinical decisions and how can neuroimaging help?. *Epilepsy Behav* 2013;**26**:313−21.
35. Giovannini G, Meletti S. Fluid biomarkers of neuro-glial injury in human status epilepticus: a systematic review. *Int J Mol Sci* 2023;**24**: 12519.
36. Thompson JA, Miralles RM, Wengert ER, Wagley PK, Yu W, Wenker IC, et al. Astrocyte reactivity in a mouse model of SCN8A epileptic encephalopathy. *Epilepsia Open* 2022;**7**:280−92.
37. Small C, Dagra A, Martinez M, Williams E, Lucke-Wold B. Examining the role of astrogliosis and JNK signaling in post-traumatic epilepsy. *Egypt J Neurosurg* 2022;**37**:1.
38. Binvignat O, Olloquequi J. Excitotoxicity as a target against neurodegenerative processes. *Curr Pharm Des* 2020;**26**:1251−62.
39. Sivakumar S, Ghasemi M, Schachter SC. Targeting NMDA receptor complex in management of epilepsy. *Pharmaceuticals* 2022;**15**:1297.
40. Reyes-Marin KE, Nuñez A. Seizure susceptibility in the APP/PS1 mouse model of Alzheimer's disease and relationship with amyloid β plaques. *Brain Res* 2017;**1677**:93−100.
41. Filali M, Lalonde R, Rivest S. Subchronic memantine administration on spatial learning, exploratory activity, and nest-building in an APP/PS1 mouse model of Alzheimer's disease. *Neuropharmacology* 2011;**60**:930−6.
42. Li DD, Zhang YH, Zhang W, Zhao P. Meta-analysis of randomized controlled trials on the efficacy and safety of donepezil, galantamine, rivastigmine, and memantine for the treatment of Alzheimer's disease. *Front Neurosci* 2019;**13**:472.
43. Schneider LS, Dagerman KS, Higgins JP, McShane R. Lack of evidence for the efficacy of memantine in mild Alzheimer disease. *Arch Neurol* 2011;**68**:991−8.
44. Prodromou C, Roe SM, O'Brien R, Ladbury JE, Piper PW, Pearl LH. Identification and structural characterization of the ATP/ADP-binding site in the Hsp90 molecular chaperone. *Cell* 1997;**90**:65−75.
45. Mohammadi-Ostad-Kalayeh S, Stahl F, Scheper T, Kock K, Herrmann C, Heleno Batista FA, et al. Heat shock proteins revisited: using a mutasynthetically generated reblastatin library to compare the inhibition of human and leishmania Hsp90s. *Chembiochem* 2018;**19**:562−74.
46. Guo W, Reigan P, Siegel D, Zirrolli J, Gustafson D, Ross D. Formation of 17-allylamino-demethoxygeldanamycin (17-AAG) hydroquinone by NAD(P)H:quinone oxidoreductase 1: role of 17-AAG hydroquinone in heat shock protein 90 inhibition. *Cancer Res* 2005;**65**:10006−15.
47. Maroney AC, Marugan JJ, Mezzasalma TM, Barnakov AN, Garrabrant TA, Weaner LE, et al. Dihydroquinone ansamycins: toward resolving the conflict between low *in vitro* affinity and high cellular potency of geldanamycin derivatives. *Biochemistry* 2006;**45**:5678−85.
48. Takatsu T, Ohtsuki M, Muramatsu A, Enokita R, Kurakata SI. Reblastatin, a novel benzenoid ansamycin-type cell cycle inhibitor. *J Antibiot (Tokyo)* 2000;**53**:1310−2.
49. Kitson RR, Chang CH, Xiong R, Williams HE, Davis AL, Lewis W, et al. Synthesis of 19-substituted geldanamycins with altered conformations and their binding to heat shock protein Hsp90. *Nat Chem* 2013;**5**:307−14.
50. Robertson N, Stratford IJ, Houlbrook S, Carmichael J, Adams GE. The sensitivity of human tumour cells to quinone bioreductive drugs: what role for DT-diaphorase?. *Biochem Pharmacol* 1992;**44**:409−12.
51. Onodera H, Kaneko M, Takahashi Y, Uochi Y, Funahashi J, Nakashima T, et al. Conformational significance of EH21A1-A4, phenolic derivatives of geldanamycin, for Hsp90 inhibitory activity. *Bioorg Med Chem Lett* 2008;**18**:1588−91.
52. Wrona IE, Gozman A, Taldone T, Chiosis G, Panek JS. Synthesis of reblastatin, autolytimycin, and non-benzoquinone analogues: potent inhibitors of heat shock protein 90. *J Org Chem* 2010;**75**:2820−35.
53. Sano F, Shigetomi E, Shinozaki Y, Tsuzukiyama H, Saito K, Mikoshiba K, et al. Reactive astrocyte-driven epileptogenesis is induced by microglia initially activated following status epilepticus. *JCI Insight* 2021;**6**:e135391.
54. Gómez-Gonzalo M, Losi G, Chiavegato A, Zonta M, Cammarota M, Brondi M, et al. An excitatory loop with astrocytes contributes to drive neurons to seizure threshold. *PLoS Biol* 2010;**8**:e1000352.
55. Yin Y, Hu J, Wu H, Yang X, Qi J, Huang L, et al. Astrocytic dopamine D1 receptor modulates glutamatergic transmission and synaptic plasticity in the prefrontal cortex through d-serine. *Acta Pharm Sin B* 2025;**15**:4692−710.
56. Sha L, Chen T, Deng Y, Du T, Ma K, Zhu W, et al. Hsp90 inhibitor HSP990 in very low dose upregulates EAAT2 and exerts potent antiepileptic activity. *Theranostics* 2020;**10**:8415−29.
57. Fu W, Lin Q, Fu Z, Yang T, Shi D, Ma P, et al. Synthesis and evaluation of TSPO-targeting radioligand [^{18}F]F-TFQC for PET neuroimaging in epileptic rats. *Acta Pharm Sin B* 2025;**15**:722−36.
58. Zhou Z, Li K, Chu Y, Li C, Zhang T, Liu P, et al. ROS-removing nanomedicine for navigating inflammatory microenvironment to enhance anti-epileptic therapy. *Acta Pharm Sin B* 2023;**13**:1246−61.
59. Jiang L, Liu N, Zhao F, Huang B, Kang D, Zhan P, et al. Discovery of GluN2A subtype-selective *N*-methyl-d-aspartate (NMDA) receptor ligands. *Acta Pharm Sin B* 2024;**14**:1987−2005.
60. Lipton SA. Paradigm shift in neuroprotection by NMDA receptor blockade: memantine and beyond. *Nat Rev Drug Discov* 2006;**5**: 160−70.
61. Tanaka K, Watase K, Manabe T, Yamada K, Watanabe M, Takahashi K, et al. Epilepsy and exacerbation of brain injury in mice lacking the glutamate transporter GLT-1. *Science* 1997;**276**: 1699−702.
62. Holmer HK, Keyghobadi M, Moore C, Menashe RA, Meshul CK. Dietary restriction affects striatal glutamate in the MPTP-induced mouse model of nigrostriatal degeneration. *Synapse* 2005;**57**:100−12.
63. Chung EK, Chen LW, Chan YS, Yung KK. Downregulation of glial glutamate transporters after dopamine denervation in the striatum of 6-hydroxydopamine-lesioned rats. *J Comp Neurol* 2008;**511**:421−37.
64. Fan S, Xian X, Li L, Yao X, Hu Y, Zhang M, et al. Ceftriaxone improves cognitive function and upregulates GLT-1-related glutamate-glutamine cycle in APP/PS1 mice. *J Alzheimers Dis* 2018;**66**: 1731−43.
65. Takahashi K, Kong Q, Lin Y, Stouffer N, Schulte DA, Lai L, et al. Restored glial glutamate transporter EAAT2 function as a potential therapeutic approach for Alzheimer's disease. *J Exp Med* 2015;**212**: 319−32.
66. Barrera-Ocampo A. Monoclonal antibodies and aptamers: the future therapeutics for Alzheimer's disease. *Acta Pharm Sin B* 2024;**14**: 2795−814.